



HAL
open science

Physics approach to the variable-mass optimal-transport problem

Patrice Koehl, Marc Delarue, Henri Orland

► **To cite this version:**

Patrice Koehl, Marc Delarue, Henri Orland. Physics approach to the variable-mass optimal-transport problem. *Physical Review E*, 2021, 103 (1), pp.012113. 10.1103/PhysRevE.103.012113. pasteur-03267961

HAL Id: pasteur-03267961

<https://pasteur.hal.science/pasteur-03267961>

Submitted on 22 Jun 2021

HAL is a multi-disciplinary open access archive for the deposit and dissemination of scientific research documents, whether they are published or not. The documents may come from teaching and research institutions in France or abroad, or from public or private research centers.

L'archive ouverte pluridisciplinaire **HAL**, est destinée au dépôt et à la diffusion de documents scientifiques de niveau recherche, publiés ou non, émanant des établissements d'enseignement et de recherche français ou étrangers, des laboratoires publics ou privés.

Copyright

Physics approach to the variable-mass optimal-transport problemPatrice Koehl¹, Marc Delarue² and Henri Orland³¹*Department of Computer Science and Genome Center, University of California, Davis, California 95616, USA*²*Unité de Dynamique Structurale des Macromolécules, Department of Structural Biology and Chemistry, UMR 3528 du CNRS, Institut Pasteur, 75015 Paris, France*³*Institut de Physique Théorique, Université Paris–Saclay, CEA, 91191 Gif/Yvette Cedex, France*

(Received 17 June 2020; revised 2 December 2020; accepted 21 December 2020; published 14 January 2021)

Optimal transport (OT) has become a discipline by itself that offers solutions to a wide range of theoretical problems in probability and mathematics with applications in several applied fields such as imaging sciences, machine learning, and in data sciences in general. The traditional OT problem suffers from a severe limitation: its balance condition imposes that the two distributions to be compared be normalized and have the same total mass. However, it is important for many applications to be able to relax this constraint and allow for mass creation and/or destruction. This is true, for example, in all problems requiring partial matching. In this paper, we propose an approach to solving a generalized version of the OT problem, which we refer to as the discrete variable-mass optimal-transport (VMOT) problem, using techniques adapted from statistical physics. Our first contribution is to fully describe this formalism, including all the proofs of its main claims. In particular, we derive a strongly concave effective free-energy function that captures the constraints of the VMOT problem at a finite temperature. From its maximum we derive a weak distance (i.e., a divergence) between possibly unbalanced distribution functions. The temperature-dependent OT distance decreases monotonically to the standard variable-mass OT distance, providing a robust framework for temperature annealing. Our second contribution is to show that the implementation of this formalism has the same properties as the regularized OT algorithms in time complexity, making it a competitive approach to solving the VMOT problem. We illustrate applications of the framework to the problem of partial two- and three-dimensional shape-matching problems.

DOI: [10.1103/PhysRevE.103.012113](https://doi.org/10.1103/PhysRevE.103.012113)**I. INTRODUCTION**

The optimal transport (OT) problem has a long history in mathematics and statistics. Originally introduced by Monge to formalize the problem of moving earth from one area to another as a linear optimization problem [1], it has been expanded as a means to handle allocation resources, and therefore it has become integral to operation research. OT, however, is not specific to applied problems. At its core, it can be seen as an option for computing the distance and a correspondence between two probability distributions (for review, see [2]). Finding such a distance and mapping between probability measures is of relevance to most, if not all data science disciplines. As such, applications of OT have exploded in recent years in domains such as signal and image processing [3–6], machine learning [7–9], computer vision and image analysis [10–15], linguistics [16,17], differential geometry [18,19], geometric shape matching [20,21], network analyses [22–24], gene expression analyses [25], and the analysis of conformational dynamics of biomolecules [26]. In addition, OT has been expanded to matrix-valued and vector-valued distributions, with applications in three-dimensional (3D) image comparisons [4,6,27,28]. For extensive reviews of OT, we recommend Refs. [2,18,29,30] for reviews on the theory, and Refs. [31,32] for reviews on its computational aspects.

A. The balanced OT problem

There are two main ways to formulate the OT problem. The traditional, static Monge-Kantorovich formulation can be expressed as follows. Let X and Y be two metric spaces, and let ρ_1 and ρ_2 be probability measures on X and Y , respectively. Let C be a cost function $C : X \times Y \rightarrow \mathbb{R}^+$. The goal is to find a probability measure G on $X \times Y$ that minimizes the total transportation cost V defined as

$$V(G) = \int_X \int_Y C(x, y) G(x, y) d(x, y). \quad (1)$$

The minimum of $T(G)$ is to be found over probability measures that satisfy the following constraints:

$$\int_Y G(x, y) dy = \rho_1(x) \quad \forall x, \quad (2a)$$

$$\int_X G(x, y) dx = \rho_2(y) \quad \forall y. \quad (2b)$$

This minimum, which we write as $\mathcal{W}(\rho_1, \rho_2)$, defines a distance between the two probability measures ρ_1 and ρ_2 [2]. This distance is referred to as the Wasserstein distance, the earth mover distance, or simply the OT distance, depending on the field of application. An alternate approach to the Monge-Kantorovich formulation is to formulate the OT problem using partial differential equations [34,35]. Within those methods, it

TABLE I. Balanced and generalized discrete OT problems.^a

Balanced OT problem ^b	Partial OT problem ^c	Generalized unbalanced OT problem ^d
$U(G) = \sum_{k,l} C(k,l)G(k,l)$	$U(G) = \sum_{k,l} C(k,l)G(k,l)$	$U(G, \mathbf{m}_1, \mathbf{m}_2) = \sum_{k,l} C(k,l)G(k,l) + D(\rho_1, \mathbf{m}_1) + D(\rho_2, \mathbf{m}_2)$
s.t. $G(k,l) \geq 0, \quad \forall k,l$ $\sum_l G(k,l) = \rho_1(k), \quad \forall k$ $\sum_k G(k,l) = \rho_2(l), \quad \forall l$	s.t. $G(k,l) \geq 0 \quad \forall k,l$ $\sum_l G(k,l) \leq \rho_1(k), \quad \forall k$ $\sum_k G(k,l) \leq \rho_2(l), \quad \forall l$ $\sum_{k,l} G(k,l) = \eta$	s.t. $G(k,l) \geq 0 \quad \forall k,l$ $\sum_l G(k,l) = m_1(k), \quad \forall k$ $\sum_k G(k,l) = m_2(l), \quad \forall l$ $\sum_k m_1(k) = \sum_l m_2(l) (= 1)$

^aOT problem between two sets of weighted points S_1 and S_2 . Each point k in S_1 is assigned a mass $\rho_1(k)$, while each point l in S_2 is assigned a mass $\rho_2(l)$. Note that ρ_1 and ρ_2 can be seen as (discrete) probability measures on S_1 and S_2 , respectively. The cost of transport between S_1 and S_2 is encoded as a positive matrix $C(k, l)$. G is the transport plan between S_1 and S_2 ; U is the total transport cost to be minimized.

^bThis is the standard balanced optimal transport under its Monge-Kantorovich formulation, with the assumption that $\sum_k \rho_1(k) = \sum_l \rho_2(l)$. See, for example, [2].

^cPartial OT problem when the probability measures ρ_1 and ρ_2 have different masses, i.e., $\sum_k \rho_1(k) \neq \sum_l \rho_2(l)$. The total mass transported is then $\eta \leq \min(\sum_k \rho_1(k), \sum_l \rho_2(l))$. See, for example, [33].

^dGeneralized OT problem in which both the transport plan G and the actual masses m_1 and m_2 that are transferred are optimized to find the minimum of a modified cost function that accounts for differences (D) between m_1 and m_2 , and the corresponding given unbalanced probability measures ρ_1 and ρ_2 (see the text for details on the definition of D).

is worth highlighting those that rely on dynamics. Brenier and Benamou [36,37] have shown that transport with quadratic costs C is equivalent to finding a time-varying sequence of distributions that smoothly interpolates between the two measures ρ_1 and ρ_2 . Their approach, initially developed from flat 2D domains, has recently been extended to discrete surfaces [38].

B. The unbalanced OT problem

It is important to realize that the traditional OT problem formulated above only applies to balanced problems. Indeed, the constraints (2) are only feasible if

$$\int_X \int_Y G(x,y)d(x,y) = \int_X \rho_1(x)dx = \int_Y \rho_2(y)dy, \quad (3)$$

namely if the two probability measures are normalized and have the same mass. This is too restrictive in many applications, as mass conservation may lead to fitting noise and outliers, and it prevents any form of partial matching. There have been significant developments to attempt to remove those restrictions and develop theories for “unbalanced,” or also referred to as partial optimal transport. There have been two main directions within those theories (for a brief summary in the discrete case, see Table I).

The first approach is to relax the constraints [Eqs. (2)] on the marginals of the transport plan G . Caffarelli and McCann [39] and Figalli [33] have proposed to minimize the transportation cost V defined in Eq. (1) under the following constraints:

$$\int_Y G(x,y)dy \leq \rho_1(x), \quad \forall x, \quad (4a)$$

$$\int_X G(x,y)dx \leq \rho_2(y), \quad \forall y, \quad (4b)$$

with the additional constraint that the total mass transported, $m = \int_X \int_Y G(x,y)d(x,y)$, be in the interval $m \in$

$[0, \min(\|\rho_1\|, \|\rho_2\|)]$, i.e., that m is positive and smaller than the total mass of ρ_1 and the total mass of ρ_2 .

The second option is to maintain the constraints on the marginals of the transport plan G , but to make those marginals a variable of the optimization process. In other words, the unbalanced distribution measures ρ_1 and ρ_2 are considered as perturbations of balanced distribution measures \mathbf{m}_1 and \mathbf{m}_2 . The cost U of transport between ρ_1 and ρ_2 can then be seen as the cost of transport between the balanced measures \mathbf{m}_1 and \mathbf{m}_2 plus the size of the perturbation:

$$U(G, \mathbf{m}_1, \mathbf{m}_2) = \int_X \int_Y C(x,y)G(x,y)d(x,y) + \tau_1 D(\rho_1, \mathbf{m}_1) + \tau_2 D(\rho_2, \mathbf{m}_2), \quad (5)$$

where τ_1 and τ_2 are two parameters, and D is a distance between two distributions. Note that \mathbf{m}_1 and \mathbf{m}_2 are now variables that are then optimized to minimize the cost $U(G, \mathbf{m}_1, \mathbf{m}_2)$. For example, Georgiou *et al.* [40] introduced this formulation to define a distance between power spectra. They set D to be the total variance between the distribution, i.e.,

$$D(\rho_1, \mathbf{m}_1) = \int_X |\rho_1(x) - m_1(x)|dx, \quad (6)$$

with a similar definition for comparing ρ_2 and \mathbf{m}_2 . Georgiou *et al.* showed that this formulation can be thought of as a transportation problem on expanded sets $X \cup \infty$ and $Y \cup \infty$ with masses added at ∞ as needed so that the two expanded sets have equal masses [40]. In addition, as the masses that are actually transferred are variable, this formalism allows for mass creation/deletion. The same ideas were further developed by Piccoli and Rossi [41,42] and Liero *et al.* [43], with variations on the choice of the distance D between distributions.

Another approach similar to the one originally proposed by Georgiou *et al.* is to use ϕ divergences for computing the perturbation between the native distributions ρ_1 and ρ_2 and the variable distribution \mathbf{m}_1 and \mathbf{m}_2 [44,45]. The most common

choice for ϕ is $\phi(t) = t \ln(t) - t + 1$, in which case D_ϕ is the Kullback-Leibler (KL) divergence:

$$\begin{aligned} D(\mathbf{m}_1, \rho_1) &= \text{KL}\left(\frac{\mathbf{m}_1}{\rho_1}\right) \\ &= \int_X \left(m_1(x) \ln\left(\frac{m_1(x)}{\rho_1(x)}\right) - m_1(x) + \rho_1(x) \right) dx. \end{aligned} \quad (7)$$

Note that the choice of Kullback-Leibler is not imposed, and many other divergences are possible [46].

C. Entropy regularized problems

The advantages of the static Monge-Kantorovich formulations of both the balanced and unbalanced OT problems are related to the fact that fast algorithms exist to solve them, making them useful in many applied problems. The existence of such fast algorithms has been triggered by the idea of minimizing regularized versions of Eqs. (1) and (5):

$$V(\epsilon, G) = V(G) - \epsilon H(G), \quad (8)$$

$$U(\epsilon, G) = U(G) - \epsilon H(G), \quad (9)$$

where ϵ is the regularization parameter, and the second term $H(G)$ is an entropic barrier that enforces the positivity of the transport plan [47]. The most common choice for $H(G)$ is an entropic regularization,

$$H(G) = - \int_X \int_Y G(x, y) [\ln(G(x, y) - 1)] dx dy, \quad (10)$$

though other regularization functions have been considered; see [32] for discussions. This regularized version of optimal transport is often called the Schrödinger problem or bridge [48–50]. It maps to the traditional balanced and unbalanced OT problems as $\epsilon \rightarrow 0$. The minima for the entropy-regularized costs $V(\epsilon, G)$ and $U(\epsilon, G)$, which we denote $\mathcal{W}_\epsilon(\rho_1, \rho_2)$ and $\mathcal{W}_{a_1, a_2, \epsilon}(\rho_1, \rho_2)$, respectively, are not distances. Indeed, it can be shown that for $\epsilon > 0$, there exists a measure γ with $\gamma \neq \rho_2$, such that $\mathcal{W}_\epsilon(\gamma, \rho_2) < \mathcal{W}_\epsilon(\rho_2, \rho_2)$ (with the same problem for $\mathcal{W}_{a_1, a_2, \epsilon}$). Note that it is possible to construct a divergence by removing the bias introduced by entropy, with the introduction of a Sinkhorn divergence $S_\epsilon(\rho_1, \rho_2)$ [51,52] associated with $\mathcal{W}_\epsilon(\rho_1, \rho_2)$:

$$S_\epsilon(\rho_1, \rho_2) = \mathcal{W}_\epsilon(\rho_1, \rho_2) - \frac{1}{2}\mathcal{W}_\epsilon(\rho_1, \rho_1) - \frac{1}{2}\mathcal{W}_\epsilon(\rho_2, \rho_2), \quad (11)$$

and similarly an unbalanced Sinkhorn divergence $S_{a_1, a_2, \epsilon}(\rho_1, \rho_2)$ [46] associated with $\mathcal{W}_{a_1, a_2, \epsilon}(\rho_1, \rho_2)$:

$$\begin{aligned} S_{a_1, a_2, \epsilon}(\rho_1, \rho_2) &= \mathcal{W}_{a_1, a_2, \epsilon}(\rho_1, \rho_2) - \frac{1}{2}\mathcal{W}_{a_1, a_2, \epsilon}(\rho_1, \rho_1) \\ &\quad - \frac{1}{2}\mathcal{W}_{a_1, a_2, \epsilon}(\rho_2, \rho_2) + \frac{\epsilon}{2}[m(\rho_1) - m(\rho_2)], \end{aligned} \quad (12)$$

where $m(\rho) = \int_X d\rho$ is the total mass of ρ .

The entropic penalization has the advantage that it defines a strongly convex problem (see [47] for the balanced OT problem, and [8,53] for the unbalanced problem). Another advantage of the regularized OT problem is that its solution

can be found efficiently through the so-called iterative proportional fitting procedure [54], also known as the Sinkhorn algorithm [55], or the Sinkhorn-Knopp algorithm [56]. Many variants of those algorithms have been developed for solving regularized balanced and unbalanced OT problems; we refer to [57–61] for overviews on those methods. Those algorithms find solutions for a given value of the relaxation parameter ϵ . For small values of this parameter, numerical issues can arise, and a stabilization of the algorithm is necessary [53]. Despite such stabilization, convergence of a stabilized Sinkhorn-Knopp algorithm can nevertheless be very slow when ϵ is small. Such small values are, however, desirable for finding good approximations to the solution of the original nonregularized OT problem, balanced or unbalanced. In addition, it is unclear whether the Sinkhorn distance is monotonic with respect to ϵ .

D. Our contribution

Our focus in this paper is to provide an alternate framework for solving the generalized OT problem in its variable-mass formulation, as derived from a statistical physics point of view, in which we fully exploit the formal analogy of the cost functions in Eq. (9) to a free energy, with ϵ an analog of a temperature, T . Such a framework has already been proposed for the Monge or assignment problem with the so-called invisible hand algorithm [62], and recently for solving the balanced OT problem [63,64]. We provide the proofs of all the properties associated with the free energy we introduce, in particular its monotonic convergence to the “true” variable-mass OT distance.

The paper is organized as follows. In Sec. II, we describe in detail the framework we propose for solving a variable-mass optimal-transport problem at finite temperature. Proofs of its major properties are provided in the Appendixes. The following section briefly describes its computational implementation. In Sec. IV, we present applications of this framework to the problems of 2D image matching and of 3D shape comparison. We limit those presentations to illustration of the performance of our framework, and we reserve comparisons with other techniques available for solving these matching problems to further studies. We finally conclude with a comparison between the entropy-regularized formulation of the unbalanced OT problem and our formalism, as well as with a discussion on future developments.

II. THE VARIABLE-MASS OPTIMAL-TRANSPORT PROBLEM AT FINITE TEMPERATURE

Let us consider a system in thermal equilibrium at a finite temperature T . This system will sample several states, with each state characterized by a probability that is related to the energy of that state. The most probable state is the one with lowest energy. Using this framework from statistical physics, minimizing an energy function can be reformulated as the problem of finding the most probable state of the system it defines. Let us apply this framework to the variable-mass discrete OT problem between two sets of points S_1 and S_2 , of size N_1 and N_2 , respectively. Each point k in S_1 (S_2) is assigned a “mass” $\rho_1(k)$ [$\rho_2(k)$]. We do not assume balance, i.e., it is possible that $\sum_k \rho_1(k) \neq \sum_l \rho_2(l)$. We encode the

cost of transport between S_1 and S_2 as a positive matrix $C(k, l)$ with $k \in \{1, \dots, N_1\}$ and $l \in \{1, \dots, N_2\}$. The “system” is then identified with the different transport plans G between S_1 and S_2 , where $G(k, l)$ is the amount of mass transferred between point k and point l . To keep the system physical, we impose that

$$G(k, l) \geq 0 \quad \forall (k, l). \quad (13)$$

In line with the concept of a generalized OT problem introduced by Georgiou *et al.* [40] and further developed by others [41,42,44,45], we consider ρ_1 and ρ_2 as perturbations of yet unknown balanced mass measures \mathbf{m}_1 and \mathbf{m}_2 set to be the marginals of the transport plan G :

$$m_1(k) = \sum_l G(k, l), \quad (14)$$

$$m_2(l) = \sum_k G(k, l), \quad (15)$$

i.e., $m_1(k)$ is the amount of mass transported from point k in S_1 by the transport plan, and $m_2(l)$ is the corresponding amount of mass received by point l in S_2 . Those masses are let free, i.e., are variables of the system, thereby allowing for mass creation/deletion. To ensure that there is mass transferred between S_1 and S_2 , we impose the constraint

$$\sum_{kl} G(k, l) = 1. \quad (16)$$

Note that the value 1 is arbitrary and could have been set to any constant, with basically no changes in the approach detailed below.

Following the concept of generalized OT for unbalanced OT (see Table I), we consider a modified energy to be optimized in which we add to the transport cost constraints on the values of the variables balanced masses \mathbf{m}_1 and \mathbf{m}_2 with respect to the given, possibly unbalanced masses ρ_1 and ρ_2 , leading to an energy for the variable-mass OT problem defined as

$$U = \sum_{kl} C(k, l)G(k, l) + \tau_1 \sum_k \left(\frac{m_1(k)}{\rho_1(k)} \right)^2 + \tau_2 \sum_l \left(\frac{m_2(l)}{\rho_2(l)} \right)^2, \quad (17)$$

where τ_1 and τ_2 are parameters. Note the similarity with the divergence formulation introduced by Chizat *et al.* [44,45]. The only difference is that we have chosen a Pearson χ^2 divergence, instead of the more traditional KL divergence, for reasons that will become clear below. To simplify notations, we rewrite this energy as

$$U = \sum_{kl} C(k, l)G(k, l) + \sum_k \alpha_1(k)m_1^2(k) + \sum_l \alpha_2(l)m_2^2(l), \quad (18)$$

where we have set $\alpha_1(k) = \tau_1/\rho_1^2(k)$ and $\alpha_2(l) = \tau_2/\rho_2^2(l)$.

Solving the variable-mass OT problem amounts to finding the transport plan G with variable marginals, as defined in Eqs. (14) and (15), which minimizes the regularized energy U defined in Eq. (18). The regularized energy associated with

this optimal transport plan will be referred to as $d_u(S_1, S_2)$ in the rest of the paper. As for the traditional, balanced OT problem, computing $d_u(S_1, S_2)$ is expensive and not scalable with respect the sizes of the point sets S_1 and S_2 . In line with the entropy regularization introduced for the balanced OT problem [47], most current solutions involve an entropy regularization to make the problem computationally tractable [53,61]. We propose an alternate solution based on statistical physics.

Each state S of the variable-mass OT system is identified with a transport plan G , vectors of masses \mathbf{m}_1 and \mathbf{m}_2 for the points in S_1 and S_2 , and its energy $U(S)$ is defined in Eq. (18). As such, the state S is represented with $N_1N_2 + N_1 + N_2$ variables. Note, however, that those variables are not independent as they are highly constrained by Eqs. (13)–(16). Note that Eq. (13) can be replaced with

$$0 \leq G(k, l) \leq 1 \quad \forall (k, l) \quad (19)$$

as a consequence of Eq. (16). Note also that we have the following constraints on the masses:

$$\sum_k m_1(k) = \sum_l m_2(l) = 1 \quad (20)$$

as a consequence of their definition, and of Eq. (16). The collection of all feasible states S is a set that we denote $\mathcal{S}(S_1, S_2)$. Note that this set is convex.

The probability distribution function for this system, $P(S)$, also referred to as the Gibbs distribution, is defined as

$$P(S) = \frac{1}{Z_\beta(S_1, S_2)} e^{-\beta U(S)}. \quad (21)$$

In this equation, $\beta = 1/(k_B T)$, where k_B is the Boltzmann constant and T is the temperature, and $Z_\beta(S_1, S_2)$ is the partition function computed over all states of the system.

This partition function is given by

$$Z_\beta(S_1, S_2) = \int_{S \in \mathcal{S}(S_1, S_2)} e^{-\beta U(S)} d\mu_{12}, \quad (22)$$

where $d\mu_{12}$ can be seen as the Lebesgue measure on $\mathcal{S}(S_1, S_2)$. The partition function Z is related to the free energy of the system by

$$\mathcal{F}_\beta(S_1, S_2) = -\frac{1}{\beta} \ln(Z_\beta(S_1, S_2)) \quad (23)$$

and to the average energy $E_\beta(S_1, S_2) = \langle U(S) \rangle_{S \in \mathcal{S}(S_1, S_2)}$ by

$$E_\beta(S_1, S_2) = -\frac{\partial \ln(Z_\beta(S_1, S_2))}{\partial \beta}. \quad (24)$$

We note first one important property of the free energy and average energy:

Property 1. For all $\beta > 0$, the free energy $\mathcal{F}_\beta(S_1, S_2)$ and the average energy $E_\beta(S_1, S_2)$ are monotonically decreasing functions of β . Both converge to the variable-mass optimal-transport distance $d(S_1, S_2)$.

Proof. The behaviors of \mathcal{F}_β and E_β with respect to β are analyzed in Appendix A.

This statistical physics formulation of the optimal transport problem is appealing. It defines a temperature-dependent free energy with a monotonic dependence on the temperature (or inverse of the temperature, β), and convergence to the actual

variable-mass optimal-transport distance at zero temperature. It is, however, of limited interest in practice as the partition function and therefore the free energy cannot be computed explicitly. We propose a scheme for approximating these quantities using the saddle point approximation. We will show that the corresponding mean-field values satisfy properties similar to the exact quantities defined above. In contrast to these exact values, we show that the mean-field values can be computed efficiently.

Taking into account the constraints that define $\mathcal{S}(S_1, S_2)$, the partition function can be rewritten as

$$\begin{aligned} Z_\beta(S_1, S_2) &= \int_0^1 \prod_{kl} dG(k, l) \int_{-\infty}^{+\infty} \prod_k dm_1(k) \int_{-\infty}^{+\infty} \prod_l dm_2(l) \\ &\times e^{-\beta[\sum_{kl} C(k, l)G(k, l) + \sum_k \alpha_1(k)m_1^2(k) + \sum_l \alpha_2(l)m_2^2(l)]} \\ &\times \prod_k \delta\left(\sum_l G(k, l) - m_1(k)\right) \\ &\times \prod_l \delta\left(\sum_k G(k, l) - m_2(l)\right) \\ &\times \delta\left(\sum_{kl} G(k, l) - 1\right). \end{aligned} \quad (25)$$

Note the limits of integrations. For the $G(k, l)$ values, they are set to be $\{0, 1\}$, based on Eq. (19). For the masses $m_1(k)$ and $m_2(l)$, we set them unconstrained in \mathbb{R} , although we know that they are positive (as sums of elements of the transport plan G that are all positive), and smaller than 1 [from Eq. (20)]. Those constraints are enforced by the δ functions.

$$\begin{aligned} Z_\beta(S_1, S_2) &= \int_{-\infty}^{+\infty} \prod_k d\lambda(k) \int_{-\infty}^{+\infty} \prod_l d\mu(l) \int_{-\infty}^{+\infty} dx \left[e^{\beta x} \int_0^1 \prod_{kl} dG(k, l) e^{-\beta \sum_{k,l} G(k, l)[C(k, l) + \lambda(k) + \mu(l) + x]} \right. \\ &\times \left. \int_{-\infty}^{+\infty} \prod_k dm_1(k) e^{-\beta[\alpha_1(k)m_1^2(k) - \lambda(k)m_1(k)]} \int_{-\infty}^{+\infty} \prod_l dm_2(l) e^{-\beta[\alpha_2(l)m_2^2(l) - \mu(l)m_2(l)]} \right]. \end{aligned} \quad (28)$$

The variables $G(k, l)$, $m_1(k)$, and $m_2(l)$ can be integrated separately. The integrals over the variables $G(k, l)$ are based on simple exponential functions, while the integrals over the masses are Gaussian integrals, with

$$\int_{-\infty}^{+\infty} e^{-\beta(\alpha x^2 - \lambda x)} dx = \sqrt{\frac{\pi}{\beta\alpha}} e^{\frac{\beta\lambda^2}{4\alpha}}. \quad (29)$$

The simplicity of the Gaussian integral is the reason that we chose Pearson's divergence in our modified energy, Eq. (18), and the ∞ limits to the integrals involving masses. Performing those integrations and ignoring the factors $\sqrt{\frac{\pi}{\beta\alpha}}$ from the Gaussian integrals, we get

$$\begin{aligned} Z_\beta(S_1, S_2) &= \int_{-\infty}^{+\infty} \prod_k d\lambda(k) \int_{-\infty}^{+\infty} \prod_l d\mu(l) \int_{-\infty}^{+\infty} dx \\ &\times e^{-\beta F_\beta(\lambda, \mu, x)}, \end{aligned} \quad (30)$$

Using Fourier analysis, we can represent a δ function as an integral of an exponential,

$$\delta(x) = \frac{1}{2\pi} \int e^{-ixt} dt, \quad (26)$$

where the integration is usually performed along the real axis. Introducing new auxiliary variables $\lambda(k)$ and $\mu(l)$, with $(k, l) \in [1, N_1] \times [1, N_2]$, and x , and omitting the inessential normalization factors $1/(2\pi)$, the partition function can be written as

$$\begin{aligned} Z_\beta(S_1, S_2) &= \int_0^1 \prod_{kl} dG(k, l) \int_{-\infty}^{+\infty} \prod_k dm_1(k) \int_{-\infty}^{+\infty} \prod_l dm_2(l) \\ &\times e^{-\beta[\sum_{kl} C(k, l)G(k, l) + \sum_k \alpha_1(k)m_1^2(k) + \sum_l \alpha_2(l)m_2^2(l)]} \\ &\times \int_{-\infty}^{+\infty} \prod_k d\lambda(k) e^{-\beta i[\sum_l \lambda(k)G(k, l) - \lambda(k)m_1(k)]} \\ &\times \int_{-\infty}^{+\infty} \prod_l d\mu(l) e^{-\beta i[\sum_k \mu(l)G(k, l) - \mu(l)m_2(l)]} \\ &\times \int_{-\infty}^{+\infty} e^{-\beta i x[\sum_{kl} G(k, l) - 1]} dx. \end{aligned} \quad (27)$$

We have factored out β for the variables $\lambda(k)$, $\mu(l)$, and x for consistency with the energy term. Similarly, note that the integrands in Z are now complex functions, while Z itself is a real number. The imaginary parts can be absorbed into $\lambda(k)$, $\mu(l)$, and x , i.e., $\lambda(k) \equiv i\lambda(k)$, $\mu(l) \equiv i\mu(l)$, and $x \equiv ix$, with now $\lambda(k)$, $\mu(l)$, and x being complex variables. Rearranging the order of integration and reorganizing the exponential terms, we get

where we have defined F_β as

$$\begin{aligned} F_\beta(\lambda, \mu, x) &= -x - \frac{1}{4} \sum_k \frac{\lambda^2(k)}{\alpha_1(k)} - \frac{1}{4} \sum_l \frac{\mu^2(l)}{\alpha_2(l)} \\ &- \frac{1}{\beta} \sum_{kl} \ln \left[\frac{1 - e^{-\beta[C(k, l) + \lambda(k) + \mu(l) + x]}}{\beta[C(k, l) + \lambda(k) + \mu(l) + x]} \right]. \end{aligned} \quad (31)$$

F_β is the functional free energy of the system. We note that it is a function of $N_1 + N_2 + 1$ variables, i.e., we have reduced the dimensionality of the problem from quadratic to linear in the number of points considered.

Let $\tilde{G}(k, l)$ be the expected value of $G(k, l)$ with respect to the Gibbs distribution given in Eq. (21). It is unfortunately not possible to compute these expected values directly from this equation, as the partition function is not known analytically.

Instead, we derive a saddle point approximation (SPA). The SPA is computed by looking for extrema of the effective free energy with respect to the variables $\lambda(k)$, $\mu(l)$, and x :

$$\frac{\partial F_\beta}{\partial \lambda(k)} = 0 \quad \frac{\partial F_\beta}{\partial \mu(l)} = 0 \quad \text{and} \quad \frac{\partial F_\beta}{\partial x} = 0. \quad (32)$$

After some rearrangements, those equations lead to the following system of equations:

$$\begin{aligned} \sum_l H(k, l) &= \frac{\lambda(k)}{2\alpha_1(k)} \quad \forall k, \\ \sum_k H(k, l) &= \frac{\mu(l)}{2\alpha_2(l)} \quad \forall l, \\ \sum_{kl} H(k, l) &= 1, \end{aligned} \quad (33)$$

where

$$H(k, l) = \phi(\beta[C(k, l) + \lambda(k) + \mu(l) + x]), \quad (34)$$

$$\phi(t) = \frac{e^{-t}}{e^{-t} - 1} + \frac{1}{t}. \quad (35)$$

The function $\phi(t)$ is defined and continuous for all real values t [with the extension that $\phi(0) = 0.5$], monotonically decreasing over \mathbb{R} , with asymptotes $y = 1$ and 0 at $-\infty$ and $+\infty$, respectively.

Note that the complex integrals defining the partition function [see Eq. (28)] do not depend on the choice of the integration paths. Equations (33) indicate that a path parallel to the real axis for each of the variables $\lambda(k)$ and $\mu(l)$ is preferred. Therefore, $\lambda(k)$ and $\mu(l)$ are real for all k and l , as is x .

Equations (33) define a nonlinear system of $N_1 + N_2 + 1$ equations, with the same number of variables. The following theorem shows that this system has a unique solution:

Theorem 1. The Hessian of the effective free energy $F_\beta(\lambda, \mu, x)$ is negative-definite. It is therefore strictly concave, and the system of Eqs. (33) has a unique solution.

Proof. See Appendix B.

In addition, we have the following property that relates the solutions of the system of equations to the expected values for the transport plan and masses transferred and received:

Property 2. Let \bar{S} be the expected state of the system with respect to the Gibbs distribution given in Eq. (21). \bar{S} is associated with an expected transport plan \bar{G} and expected masses $\bar{\mathbf{m}}_1$ and $\bar{\mathbf{m}}_2$. Let λ^{MF} , μ^{MF} , and x^{MF} be the unique solutions of the system of Eqs. (33). Then the following identities hold:

$$\begin{aligned} \bar{G}(k, l) &= \phi(\beta[C(k, l) + \lambda^{\text{MF}}(k) + \mu^{\text{MF}}(l) + x^{\text{MF}}]), \\ \bar{m}_1(k) &= \frac{\lambda^{\text{MF}}(k)}{2\alpha_1(k)}, \quad \bar{m}_2(l) = \frac{\mu^{\text{MF}}(l)}{2\alpha_2(l)}. \end{aligned}$$

Note that the solutions are mean-field solutions, hence the superscript ‘‘MF’’

Proof. See Appendix C.

For a given value of the parameter β , the expected values $\bar{G}(k, l)$ that are solutions to the system of Eqs. (33) form

a transport plan G_β^{MF} between S_1 and S_2 that is optimal with respect to the free energy defined in (31). Similarly, $\bar{\mathbf{m}}_1 = \mathbf{m}_1^{\text{MF}}$ and $\bar{\mathbf{m}}_2 = \mathbf{m}_2^{\text{MF}}$ are the optimal masses transferred from, and received by, S_1 and S_2 , respectively. We can associate these values with an optimal free energy F_β^{MF} and an optimum energy $U_\beta^{\text{MF}} = \sum_{k,l} G_\beta^{\text{MF}}(k, l)C(k, l) + \sum_k \alpha_1(k)[m_1^{\text{MF}}(k)]^2 + \sum_l \alpha_2(l)[m_2^{\text{MF}}(l)]^2$. Note that those two values are the mean-field approximations of the exact free energy and internal energy defined in Eqs. (23) and (24), respectively. We now list important properties of U_β^{MF} and F_β^{MF} .

Property 3. F_β^{MF} and U_β^{MF} are monotonically decreasing functions of the parameter β . In addition, both converge to the optimal variable-mass transport energy $d_u(S_1, S_2)$.

Proof. The monotonicities of F_β^{MF} and U_β^{MF} are established in Appendixes D and E, respectively.

In contrast with the corresponding values for the balanced OT problem [63,64], the converged optimal variable-mass transport energy $d_u(S_1, S_2)$ does not define a distance as it does not satisfy the triangular inequality. Indeed, let us consider two arbitrary sets of points S_1 and S_2 , and a combined set $S_3 = S_1 \cup S_2$. Both U^{MF} and F^{MF} will be small when comparing S_1 and S_3 and when comparing S_2 and S_3 , while they may be large when comparing S_1 with S_2 , as those sets are arbitrary. This is a common issue with partial matching. Note that the balanced OT distances between S_1 and S_3 , and between S_2 and S_3 , are likely to be large to allow for mass transfer over the whole set S_3 , which is not the desired behavior when comparing sets that may only have partial matching. The framework proposed here solves this problem. Note also that U^{MF} and F^{MF} are not even divergences, as they are not zero when comparing a set with itself. This can easily be corrected by following an idea proposed by Peyré and collaborators [46,58] and defining

$$\begin{aligned} SU_\beta(S_1, S_2) &= U_\beta^{\text{MF}}(S_1, S_2) \\ &\quad - 0.5[U_\beta^{\text{MF}}(S_1, S_1) + U_\beta^{\text{MF}}(S_2, S_2)], \\ SF_\beta(S_1, S_2) &= F_\beta^{\text{MF}}(S_1, S_2) \\ &\quad - 0.5[F_\beta^{\text{MF}}(S_1, S_1) + F_\beta^{\text{MF}}(S_2, S_2)]. \end{aligned} \quad (36)$$

Theorem 1 and the proposition 3 above highlight a number of advantages of the proposed framework that rephrases the variable-mass transport problem as a temperature-dependent process. First, at each temperature the variable-mass transport problem is turned into a strongly concave problem with a unique solution. This problem has a linear complexity in the number of variables, compared to the quadratic complexity of the original problem. The concavity allows for the use of simple algorithms for finding a minimum of the effective free-energy function [Eq. (31)]. We note also that Eqs. (33) provide good numerical stability for computing the transport plan because of the ratio of exponentials. Second, the convergence as a function of temperature is monotonic. Note, however, that in contrast with the corresponding values for the balanced OT problem [63,64], they do not define distances as they do not satisfy the triangular inequality.

Algorithm 1 *FreeOT*: a temperature-dependent framework for computing the Optimal Transport Distance between two weighted set of points

Input: The two sets of points S_1 and S_2 and the cost matrix C between S_1 and S_2 . Initial value β_0 for β

Initialize: Initialize arrays λ and μ to 0, and initialize $x = 0$. Set $STEP = \sqrt{10}$. Set $\beta^0 = \beta_0/STEP$

for $k = 1, \dots$ until convergence **do**

(1) Initialize $\beta^k = STEP * \beta^{k-1}$.

(2) Solve nonlinear Eqs. (33) for λ , μ , and x at saddle point

(3) Compute optimal transport plan G_β^{MF} , masses \mathbf{m}_1^{MF} , \mathbf{m}_2^{MF} , and $U^{MF}(\beta^k)$

(4) Check for convergence: if $|U^{MF}(\beta^k) - U^{MF}(\beta^{k-1})|/U^{MF}(\beta^{k-1}) < TOL$, stop

end for

Output: The converged transport plan $G_\beta^{MF}(k, l)$, masses \mathbf{m}_1^{MF} , \mathbf{m}_2^{MF} , and the corresponding transport cost $U^{MF}(\beta)$.

III. IMPLEMENTATION

We have implemented the finite-temperature optimal transport framework described here in a C++ program FREEOT that is succinctly described in Algorithm 1.

FREEOT is based on an iterative procedure in which the parameter β (inverse of the temperature) is gradually increased. At each value of β , the nonlinear system of equations defined by Eqs. (33) is solved using an iterative Newton-Raphson method. At each iteration for this Newton method, the Jacobian of the system of equations is computed, and a linear system is solved based on this Jacobian, whose solution provides estimates for the arrays of parameters λ and μ . These new estimates are then used to assess how well the SPA equations are satisfied. Once the errors on the SPA equations fall below a tolerance TOL (usually set to 10^{-8}), the optimal transport plan G_β^{MF} and the corresponding transport energy $U^{MF}(\beta)$ are computed. If the latter falls within the tolerance TOL of the corresponding value computed for the previous β value, the procedure is deemed to have converged and the program is stopped. Note that the converged values of λ , μ and x at a given β serve as input for the following β .

The variable-mass OT algorithm described here is as straightforward to implement as the balanced counterpart. As described in Sec. III and in Ref. [64] for the balanced version, its main computing cost is associated with solving the nonlinear set of equations corresponding to the SPA at each value of β . As mentioned above, we solve this system of equations using an iterative Newton-Raphson method that requires solving a linear system of equations based on the Jacobian of the nonlinear equations. We considered two methods for solving this system. First, we use a direct method with which we decompose the matrix describing the system using a LDL decomposition, as implemented in the program DSYSV from the LAPACK packages [65]. The corresponding time complexity is expected to be $O(N^3)$. Second, we implemented an iterative conjugate gradient (CG) method (see Appendix F). Each iteration of the CG methods involves two matrix-vector multiplications, which are of order $O(N^2)$. The CG method will converge in at most N iterations, and in many cases in many fewer iterations. As such, it is expected to be faster than the direct method if the total number of CG iterations is small. In all cases described below, we have indeed observed an apparent time complexity of $O(N^2)$ for the iterative CG method. The same behavior was observed when solving the traditional balanced OT problem [64].

IV. COMPUTATIONAL EXPERIMENTS

A. Partial 2D image matching

We present some computational examples that illustrate the use of our framework for 2D image comparison. We used the publicly available Mythological Creatures 2D database [66], to which we added a collection of scissors from the 2D Tools database [66]. Our database comprises 20 binary images corresponding to 20 shapes, 5 men, 5 horses, 5 centaurs, and 5 scissors. The shapes within one group (men, horses, centaurs, or scissors) differ by an articulation and additional parts. We characterized each image by selecting a set of “keypoints” using the ORB procedure. ORB is an image feature detector and descriptor used for object recognition and image registration [67]. Within ORB, a keypoint is a pixel within the image that is expected to be significant, i.e., a signature feature of the image. The significance is defined from a local neighborhood of the pixel of interest, characterized by a vector of 64 features. The distance between two keypoints is then defined as the Euclidean distance between their feature vectors. We use this representation to compare images in our database. A pair of images is represented with their sets of keypoints, S_1 and S_2 , the cost matrix C between those keypoints, such that $C(k, l)$ between a keypoint k on image 1 and a keypoint l on image 2 is equal to the Euclidean distance between their feature vectors. The given masses ρ and σ of the keypoints are set to 1. Note that as the number of keypoints in the two images can be different, the total masses $\sum_k \rho(k)$ and $\sum_l \sigma(l)$ can be different, and therefore this falls into the category of unbalanced OT. The masses \mathbf{m}_1 and \mathbf{m}_2 of the keypoints on the two images are left variables. In all comparisons, we set the weights of the mass regularization $\tau_1 = \tau_2 = 50$ [see Eq. (17)].

In Fig. 1, we illustrate the effectiveness of our variable-mass OT framework in identifying partial match by showing the results of the comparisons of a man and a centaur, and of the same centaur and a horse. ORB keypoints for those images are shown as circles whose radii relate to the size of the corresponding meaningful neighborhoods. A line between two keypoints k and l from two different images indicates that the value of the optimized transport between k and l , $G_\beta^{MF}(k, l)$, is greater than a threshold, set to 0.01. As expected, connections between the man and the centaur are found at the level of their heads and shoulder, while connections between the centaur and the horse are found at the level of their legs and tails. Note the two spurious links between one of the man’s

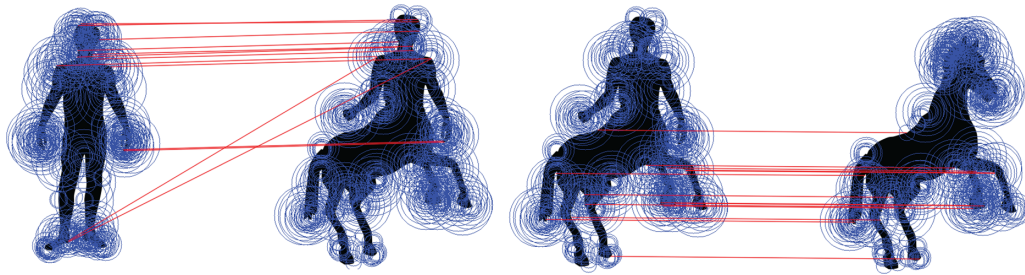


FIG. 1. Partial matchings using our variable-mass OT framework between the image of a man and the image of a centaur (left) and between the image of the same centaur and the image of a horse (right).

feet, and the neck of the centaur. Those lines relate to similar curvatures within the corresponding regions.

We then computed two score matrices $D(\infty)$, one based on balanced OT [64], $D_{OT}(\infty)$, and one based on the variable-mass OT framework described here, $D_{VMOT}(\infty)$. For the balanced OT case, $D_{OT}(\infty)(k, l)$ is the optimized transport energy $U^{MF}(G_{MF})$, i.e., the temperature-based distance between the sets of keypoints S_k and S_l of the images k and l at convergence with respect to β , usually $\beta = 10^{10}$. For the variable-mass OT case, we compute the equivalent optimized transport energy $U^{MF}(G_{MF})$ at convergence with respect to β , but we set $D_{VMOT}(\infty)$ to the corresponding divergence value SU , as defined in Eq. (36). Figure 2 depicts the difference between those two matrices. The matrix $D_{OT}(\infty)$ relates to global matching between the shapes. It shows four clusters corresponding to the four types of shapes. While it does show some level of similarity between centaurs and horses, it puts the men far from those, as far as the unrelated scissors. In contrast, $D_{VMOT}(\infty)$, which relates to partial matching between the shapes, does identify that the centaurs share similarities with horses and with men, while still being significantly distinct from scissors.

B. Partial 3D point registration

In the section above, we have illustrated the effectiveness of our framework on the problem of partial 2D image

matching. Here we look at the equivalent problem of matching 3D shapes represented by point clouds.

Rigid point cloud registration, also known as point set registration, is the process of finding a spatial rigid body transformation (e.g., scaling, rotation, and translation) that aligns two point clouds. As a special case, the two point clouds have the same cardinality, and the correspondence between the points is known. The registration problem is then limited to finding the optimal rigid body transformation that aligns the corresponding points; this is the so-called Procrustes problem for which many solutions have been proposed [68]. The general point cloud registration problem, however, is more complex as the points may have different cardinality, leading to partial registration, and the correspondence, i.e., the list of equivalent points in the two clouds, is often not known. Indeed, the correspondence is part of the desired output, along with the optimal transformation. The point cloud registration problem can then be stated as finding the maximal subsets of the two point clouds that exhibit the highest degree of similarity. Many algorithms have been proposed to solve this problem (see, for example, Refs. [69,70]), with the iterative closest point (ICP) algorithm [71] and its variations still being the most popular. In the ICP algorithm, one point cloud, the target, S_1 is kept fixed, while the other one, the source, S_2 is transformed to best match the target. The algorithm proceeds in an iterative fashion by alternating in (i) given the transformation, finding the closest point in T for every point in

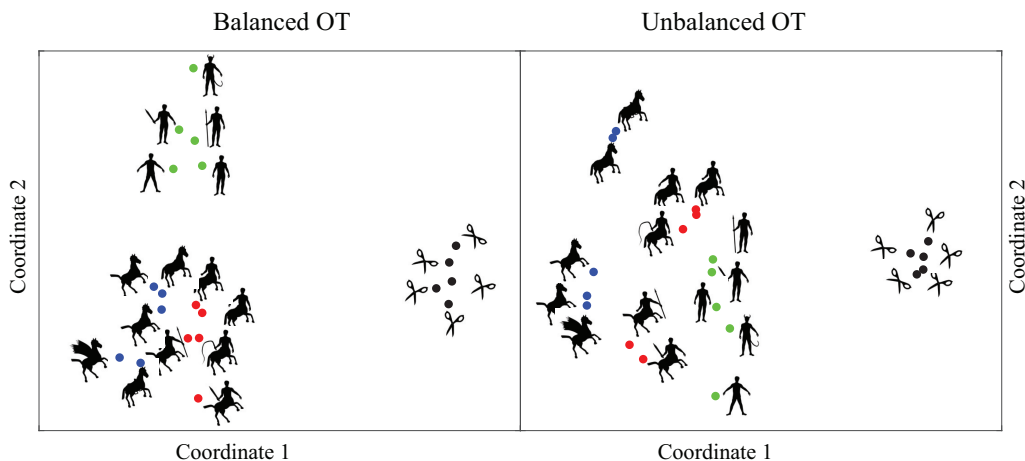


FIG. 2. Visualization of global similarity (balanced OT distance, left) and partial similarity (variable-mass OT distance, right) between the mythical creatures and the scissors. The distance matrices corresponding to all-against-all comparisons of the different shapes are projected onto the 2D plane using multidimensional scaling. Coordinate 1 and Coordinate 2 are arbitrary coordinates in this 2D plane.

S ; and (ii) given the correspondences from (i), finding the best rigid transformation by solving the Procrustes problem. Our approach differs as we propose to identify the correspondence and the transformation R directly by solving the following minimization problem:

$$R^{\text{opt}} = \operatorname{argmin}_R d_{\text{OT}}(S_1, R(S_2)), \quad (37)$$

where $R(S_2)$ refers to the positions of the points in S_2 after application of the transformation R , and d is either the balanced or variable-mass optimal-transport cost between S_1 and the transformed S_2 . We compute d as U_{∞}^{MF} , i.e., at convergence with respect to β , using the framework presented in [64] for the balanced OT cost, and using the framework presented in this paper for the variable-mass OT cost. We refer to those values as $U_{\text{OT}}^{\text{MF}}$ and $U_{\text{VMOT}}^{\text{MF}}$ for the balanced and variable-mass case, respectively. In both formulations, the cost matrix C is based on the Euclidean distances between points in S_1 and points in S_2 after application of the transformation R . In the balanced case, the masses of the points are set uniform, while in the variable-mass case these masses are variable. We solve the minimization problem in Eq. (37) using the limited memory BFGS algorithm [72].

This algorithm starts with an initial estimate of the optimal value, R^0 , and proceeds iteratively to refine that estimate with a sequence of better estimates (R_1, R_2, \dots). The derivatives g of the function d with respect to the parameters of the transformation R are used to identify the direction of steepest descent, and also to form an estimate of the Hessian matrix of second derivatives. As only the cost matrix C is an explicit function of R , we evaluate the derivatives of d with respect to the different $C(k, l)$ for all $(k, l) \in [1, N_1] \times [1, N_2]$. We show the calculation for $d = U_{\text{VMOT}}^{\text{MF}}$; the same reasoning applies for $U_{\text{OT}}^{\text{MF}}$. Recall that

$$U_{\text{VMOT}}^{\text{MF}} = \sum_{kl} C(k, l) G^{\text{MF}}(k, l) + \frac{1}{4} \sum_k \frac{[\lambda^{\text{MF}}(k)]^2}{\alpha_1(k)} + \frac{1}{4} \sum_l \frac{[\mu^{\text{MF}}(l)]^2}{\alpha_2(l)}, \quad (38)$$

where $G^{\text{MF}}(k, l)$, the optimal transport plan, is a function of the optimized values λ^{MF} , $\mu^{\text{MF}}(l)$, and x^{MF} (see Sec. II above). The energy functions U_{OT} and U_{VMOT} are therefore functions

of the cost matrix C and of the unconstrained variables λ , μ , and x . Using the chain rule,

$$\begin{aligned} \frac{dU_{\text{VMOT}}^{\text{MF}}}{dC(k, l)} &= \frac{\delta U_{\text{VMOT}}^{\text{MF}}}{\delta C(k, l)} + \sum_k \frac{\delta U_{\text{VMOT}}^{\text{MF}}}{\delta \lambda(k)} \frac{\delta \lambda(k)}{\delta C(k, l)} \\ &+ \sum_l \frac{\delta U_{\text{VMOT}}^{\text{MF}}}{\delta \mu(l)} \frac{\delta \mu(l)}{\delta C(k, l)} + \frac{\delta U_{\text{VMOT}}^{\text{MF}}}{\delta x} \frac{\delta x}{\delta C(k, l)}. \end{aligned} \quad (39)$$

A key simplification to computing the corresponding derivatives comes from the properties of the energy at the mean field. In Appendix E, we have shown that

$$\frac{\delta U_{\text{VMOT}}^{\text{MF}}}{\delta \lambda(k)} = \frac{\delta U_{\text{VMOT}}^{\text{MF}}}{\delta \mu(l)} = \frac{\delta U_{\text{VMOT}}^{\text{MF}}}{\delta x} = 0 \quad (40)$$

for all (k, l) . From those properties, we derive that

$$\frac{dU_{\text{VMOT}}^{\text{MF}}}{dC(k, l)} = \frac{\delta U_{\text{VMOT}}^{\text{MF}}}{\delta C(k, l)} = G^{\text{MF}}(k, l). \quad (41)$$

We can show using similar properties that

$$\frac{dU_{\text{OT}}^{\text{MF}}}{dC(k, l)} = G^{\text{MF}}(k, l). \quad (42)$$

As C is directly computed from the transformation R , the derivatives of C with respect to the parameters of R are computed using the chain rule. The transformation R is defined by three rotations r_x, r_y , and r_z , three translations t_x, t_y , and t_z , and a scaling factor s . The rotations are represented using the exponential map [73].

In Fig. 3, we illustrate the differences between balanced OT and VMOT when used for matching 3D shapes following the algorithm described above. Our test set is SPOT, a spotted cow (courtesy of Crane's laboratory), whose triangulated surface mesh was undersampled such that it contains 498 vertices and 992 faces. Note that while SPOT is provided as a triangulated mesh, we only consider its vertices that form the target point cloud, S_1 . We reordered those vertices such that the first 184 form the head of SPOT. The same 184 vertices constitute the source data set S_2 . We initialized the position of S_2 far from S_1 [see Fig. 3(a)] and estimated the similarity transform between them using the algorithm above under two settings,

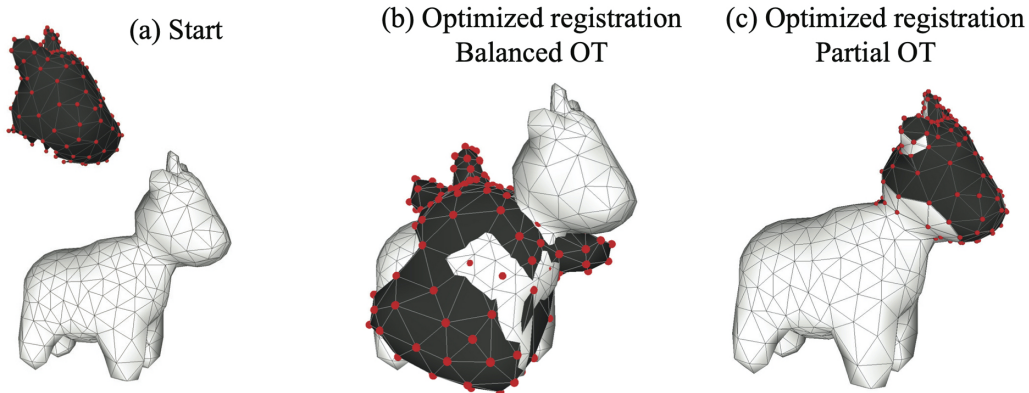


FIG. 3. We register the head of SPOT (black, with red dots at the vertices) to the full SPOT using an optimization of the rigid body transformation based on either balanced optimal transport (right) or variable-mass optimal transport (center).

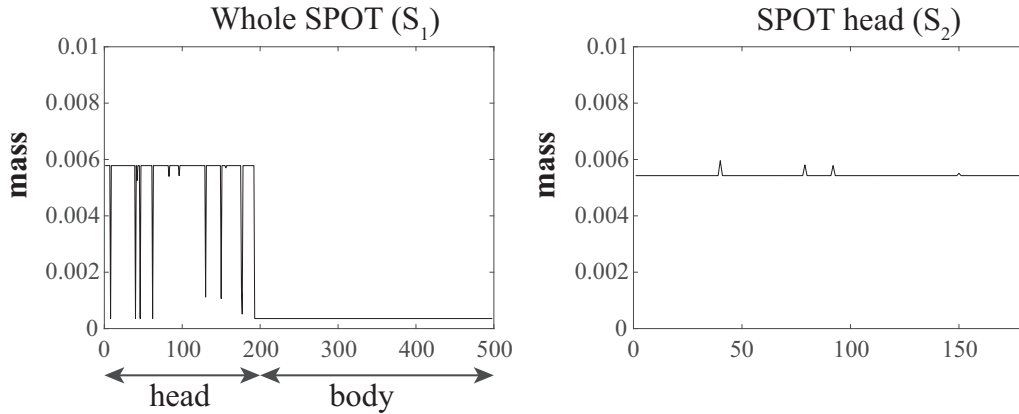


FIG. 4. Optimized masses of the points in S_1 , the full SPOT, and in S_2 , SPOT’s head, after registration of the two datasets using variable-mass optimal transport.

first using the balanced OT distance and second using the partial OT framework developed in this paper. The corresponding converged positions of S_2 with respect to S_1 are shown in Figs. 3(b) and 3(c), respectively. The balanced OT framework assumes that masses are transferred from all points in S_1 , and received by all points in S_2 , thereby imposing a global registration of the two sets of points. As a consequence, the head formed by S_2 is translated toward the center of mass of S_1 , and rotated and scaled up such that it provides a maximum coverage of the points in S_1 . In contrast, under the variable-mass OT framework, the amount of masses transported from each point in S_1 and received by each point in S_2 is adapted to minimize the regularized energy described by Eq. (18), leading to good performance and nearly perfect match of S_2 onto the head of SPOT within S_1 . To further illustrate the importance of leaving the masses variable, we show in Fig. 4 the converged masses of the points in S_1 (whole SPOT) and of the points in S_2 (SPOT’s head). While only the first points in S_1 have nonzero masses (i.e., those points that correspond to the head), all points in S_2 received some masses. Note that the registration is not perfect, as some points among the head of the whole SPOT do not have correspondence in S_2 .

V. DISCUSSION

Applications of statistical physics to solve an optimal transport problem are not new. Probably the first method using physics is the “invisible hand algorithm” [62], which solves the assignment problem, namely the Monge formulation of the OT problem in which the transport plan is binary. Recently, we proposed [63,64] an extension of the invisible hand algorithm for solving the relaxed Monge-Kantorovich version of the OT problem, in which the transport plan is now real, continuous, with fixed marginals corresponding to the fixed masses of the sets of points being compared. This paper deals with an even more relaxed version of the OT problem in which the masses are left variable. We refer to this problem as VMOT, for variable-mass OT. The solution we implemented is very similar to the one we proposed for the balanced OT problem with fixed masses. Given two sets of points S_1 and S_2 , and a cost matrix between those sets, solving VMOT is to find a transport plan G between S_1 and S_2 with variable

marginals that minimize the cost of mass transport between the two sets. The masses are left variable but the total mass transported is kept fixed. The VMOT problem is based on a regularized version of the transfer cost, to reduce the risk of finding trivial solutions with masses concentrated on one point in each set. We solve this problem by considering the partition function over all possible transfer plans between S_1 and S_2 . While the corresponding free energy cannot be computed exactly, it can be estimated using a saddle point approximation. The saddle point approximation is derived by constructing a strictly concave effective energy function that captures the constraints of the variable-mass optimal-transport problem. This effective energy function is parametrized by temperature. Its maximum defines an optimal transport plan, whose row and column marginals correspond to the masses transferred by S_1 , and received by S_2 , respectively. We proved that this energy decreases monotonically as a function of β (the inverse of temperature) to the variable-mass regularized optimal transfer cost, providing a robust framework for temperature annealing. We described an application of our framework for 3D partial matching between point clouds.

The framework we propose falls within one of the three categories of “partial OT problems,” as described in the Introduction, i.e., a formulation that allows for mass creation/destruction. In practice, this means that the masses of the points representing the distributions to be compared are not given as input, but become variables of the problem. The mass transport remains “balanced,” namely there is as much mass leaving the distribution 1 as there is mass reaching the distribution 2, as illustrated by Eq. (20). By letting the individual masses be variable, we are able to detect partial matches between the distribution. This formulation, however, has one serious limitation, as by construction it cannot handle comparison of weighted points with known weights. We are currently working on a new framework that would solve this problem of partial matching between weighted points.

It is worth comparing our approach to solving the VMOT with the entropy-regularized approach originally introduced for solving the balanced OT problem by Cuturi [47], and later extended to the unbalanced problem (see, for example, [43–45]). Both approaches consider a regularized cost or

energy function of the form

$$U_{\text{VMOT}} = \sum_{kl} C(k, l)G(k, l) + D_\phi\left(\frac{\mathbf{G}_{S_1}}{\boldsymbol{\rho}_1}\right) + D_\phi\left(\frac{\mathbf{G}_{S_2}}{\boldsymbol{\rho}_2}\right),$$

where $\boldsymbol{\rho}_1$ and $\boldsymbol{\rho}_2$ are reference mass vectors for S_1 and S_2 (often uniform mass distributions, as in the examples shown above), \mathbf{G}_{S_1} is the marginal of G projected on S_1 , i.e., $G_{S_1}(k) = \sum_l G(k, l)$, G_{S_2} the marginal of G projected on S_2 , and D_ϕ is a ϕ divergence. The most common choice for ϕ in the entropy-regularized formulation of VMOT is $\phi(t) = t \ln(t) - t + 1$, in which case D_ϕ is the Kullback-Leibler (KL) divergence. In our formulation, we use instead $\phi(t) = t^2 - 1$, i.e., a Pearson χ^2 divergence. There is one additional constraint on the values $G(k, l)$, namely their positivity. This constraint is incorporated into the energy in the entropy regularization by adding an entropy term,

$$F(\epsilon) = U_{\text{VMOT}} - \epsilon \left(- \sum_{kl} G(k, l) \ln(G(k, l)) \right),$$

where ϵ is a parameter. From a scientific computing point of view, the additional term is equivalent to adding a barrier that enforces positivity of the $G(k, l)$. As such, it falls under the category on barrier function methods that are standard techniques for solving linear and nonlinear optimization problems [74]. For the OT and VMOT problems, this formulation allows for computationally fast solutions as the energy F is convex and its minimum can be found using the Sinkhorn algorithm [55] or one of its variants with a time complexity of $O(N^2)$ (see, for example, Ref. [61] for an analysis of the Sinkhorn algorithm applied to the VMOT problem). From a physics point of view, the problem of minimizing the energy U_{VMOT} has been replaced with the problem of optimizing a “free energy” $F(\epsilon)$ where ϵ plays the role of temperature. Our approach is conceptually similar: we also introduce a free energy, concave in our case, whose optimum can be found efficiently with a time complexity of $O(N^2)$ on average [and $O(N^3)$ in the worst case]. From a computational point of view, however, our implementation is proved to be more stable and allow for convergence even at very low temperature (high β values), due to the well-behaved function ϕ that relates the unconstrained variables λ , μ , and x (which can be seen as Lagrange multipliers) and the solution G to the optimization problem.

We have described a simple application of our framework to the problem of partial matching of 3D shapes. We note, however, that this is still preliminary, as there are many problems that still need to be solved. First, the method as described only considers the vertices of the meshes representing the shapes, thereby ignoring the idea of “shapes” and only considering point clouds. Second, as all iterative methods designed to solve a nonlinear optimization problem, the success of our method is strongly dependent on its initialization, i.e., on the choice of the initial parameters. We are currently working on expanding our method to address those two problems.

Finally, we note that the variable-mass OT problem considered in this paper assumes that the two sets of points

considered are embedded in the same metric space, namely that we can build the cost matrix C that connects them. Situations in which the points lie in different, unregistered metric spaces have led to an extension to the optimal transport problem with the notion of Gromov-Wasserstein distances between metric measured spaces [75]. We believe that the concept of finite-temperature variable-mass optimal transport can be extended in the same way into a finite-temperature variable-mass Gromov-Wasserstein cost. We are currently working on this problem.

ACKNOWLEDGMENTS

The work discussed here originated from a visit by P. K. at the Institut de Physique Théorique, CEA Saclay, France. He thanks them for their hospitality and financial support. P.K. acknowledges support from NSF Award No. 1760485.

APPENDIX A: PROOF OF PROPERTY 1: MONOTONICITY OF THE FREE ENERGY AND AVERAGE ENERGY

Let us consider two sets of points S_1 and S_2 of sizes N_1 and N_2 in a metric space \mathcal{M} with given (unbalanced) masses $\boldsymbol{\rho}_1$ and $\boldsymbol{\rho}_2$, and associated (variable)-mass vectors \mathbf{m}_1 and \mathbf{m}_2 , respectively. We characterize this system with a cost matrix C and a transport polytope $\mathcal{S}(S_1, S_2)$. Recall that any state $S = (G, \mathbf{m}_1, \mathbf{m}_2)$ in this polytope satisfies the four conditions in Eqs. (14), (15), (16), and (19). It is associated with a cost $T(S)$ and an energy $U(S)$, defined as

$$T(S) = \sum_{kl} C(k, l)G(k, l), \tag{A1}$$

$$U(S) = \sum_{kl} C(k, l)G(k, l) + \sum_k \alpha_1(k)m_1^2(k) + \sum_l \alpha_2(l)m_2^2(l), \tag{A2}$$

where $\alpha_1(k) = \tau_1/\rho_1^2(k)$ and $\alpha_2(l) = \tau_2/\rho_2^2(l)$, and τ_1 and τ_2 are parameters. Note that $U(S)$ is a regularized version of $T(S)$ that includes divergences on how the marginals \mathbf{m}_1 and \mathbf{m}_2 differ from uniform distributions.

We first prove that the volume of the transport polytope $\mathcal{S}(S_1, S_2)$ is smaller than 1. Note that all the $G(k, l)$, $m_1(k)$, and $m_2(l)$ are constrained to be in the interval $[0, 1]$. The volume of the polytope is

$$\begin{aligned} & \text{Vol}(\mathcal{S}(S_1, S_2)) \\ &= \int_{S \in \mathcal{S}(S_1, S_2)} d\mu_{ij} \\ &= \int_0^1 \prod_{kl} dG(k, l) \int_0^1 \prod_k dm_1(k) \int_0^1 \prod_l dm_2(l) \\ & \times \prod_k \delta\left(\sum_l G(k, l) - m_1(k)\right) \\ & \times \prod_l \delta\left(\sum_k G(k, l) - m_2(l)\right) \\ & \times \prod_{kl} \delta\left(\sum_{kl} G(k, l) - 1\right). \end{aligned} \tag{A3}$$

As the $G(k, l)$, $m_1(k)$, and $m_2(l)$ are integrated between 0 and 1, and as the constraints set by the δ functions restrain the space of possible states, we have indeed that $0 \leq \text{Vol}(\mathcal{S}(S_1, S_2)) \leq 1$.

The free energy \mathcal{F}_β of this system is related to its internal energy E_β and entropy S_β through the general relation $\mathcal{F}_\beta = E_\beta - TS_\beta$, where T is the temperature and $\beta = 1/(k_B T)$.

The internal energy is the thermodynamic average of the regularized energy U [see Eq. (A2)] and is given by

$$E_\beta = \langle U(S) \rangle_{S \in \mathcal{S}(S_1, S_2)} = \frac{d(\beta \mathcal{F}_\beta)}{d\beta} \quad (\text{A4})$$

while the entropy is given by

$$S_\beta = \beta^2 \frac{d\mathcal{F}_\beta}{d\beta} = -\frac{d\mathcal{F}_\beta}{dT}. \quad (\text{A5})$$

An important implication of these relations is that

$$\frac{dE_\beta}{d\beta} = -(\langle U^2 \rangle - \langle U \rangle^2), \quad (\text{A6})$$

where the thermodynamic averages $\langle \cdot \rangle$ are computed over the polytope $\mathcal{S}(S_1, S_2)$. The quantity on the left is minus the variance of the energy and is therefore negative for all values of β . As a result, the internal (or average) energy of the system decreases as β increases. As $U(S)$ is positive (as the cost matrix C and the transportation plan G are positive, and the regularization terms for masses are also positive), E_β is positive: it has a limit when $\beta \rightarrow \infty$. This limit is the optimal variable-mass transport cost $d_u(S_1, S_2)$.

The entropy is negative. Indeed, the total number of states at an energy U^0 is given by

$$\begin{aligned} \mathcal{N}(U^0) &= e^{S_\beta(U^0)} \\ &= \int_{P \in \mathcal{S}(S_1, S_2)} \delta(U^0 - U(S)) d\mu_{ij}. \end{aligned} \quad (\text{A7})$$

As the volume of the polytope $\mathcal{S}(S_i, S_j)$ is smaller than 1 (see above),

$$\mathcal{N}(U^0) = e^{S_\beta(U^0)} \leq 1 \quad (\text{A8})$$

and therefore $S_\beta(U^0) \leq 0$. As this is true for all values of U , we have $S_\beta(T) \leq 0 \quad \forall T$. The free energy is related to the entropy by

$$\frac{d\mathcal{F}_\beta}{dT} = -\beta^2 \frac{d\mathcal{F}_\beta}{d\beta} = -S_\beta(T). \quad (\text{A9})$$

Therefore,

$$\frac{d\mathcal{F}_\beta}{d\beta} = \frac{S_\beta(T)}{\beta^2} \leq 0. \quad (\text{A10})$$

Therefore, the free energy of the system decreases as β increases. Its limit for $\beta \rightarrow \infty$ is the same as the limit of E_β , namely the optimal variable-mass transport cost $d_u(S_1, S_2)$.

APPENDIX B: PROOF OF THEOREM 1: CONCAVITY OF THE EFFECTIVE FREE ENERGY

We show that the effective free energy is concave by establishing that its Hessian H is negative-definite.

Recall that the effective free energy at a state $P = (G, m_1, m_2)$ is given by

$$\begin{aligned} F_\beta(\boldsymbol{\lambda}, \boldsymbol{\mu}, x) &= -x - \frac{1}{4} \sum_k \frac{\lambda^2(k)}{\alpha_1(k)} - \frac{1}{4} \sum_l \frac{\mu^2(l)}{\alpha_2(l)} \\ &\quad - \frac{1}{\beta} \sum_{kl} \ln \left[\frac{1 - e^{-\beta[C(k, l) + \lambda(k) + \mu(l) + x]}}{\beta[C(k, l) + \lambda(k) + \mu(l) + x]} \right]. \end{aligned} \quad (\text{B1})$$

$F_\beta(\boldsymbol{\lambda}, \boldsymbol{\mu}, x)$ is a function of $N_1 + N_2 + 1$ variables, the values $\lambda(l)$ are associated with the constraints on the N_1 points of set S_1 , the values $\mu(l)$ are associated with the constraints on the N_2 points of set S_2 , and the value x is associated with the constraint (16). Its derivatives with respect to those variables are

$$\begin{aligned} \frac{\partial F_\beta(\boldsymbol{\lambda}, \boldsymbol{\mu}, x)}{\partial \lambda(k)} &= \sum_l G(k, l) - \frac{\lambda(k)}{2\alpha_1(k)}, \\ \frac{\partial F_\beta(\boldsymbol{\lambda}, \boldsymbol{\mu}, x)}{\partial \mu(l)} &= \sum_k G(k, l) - \frac{\mu(l)}{2\alpha_2(l)}, \\ \frac{\partial F_\beta(\boldsymbol{\lambda}, \boldsymbol{\mu}, x)}{\partial x} &= \sum_{kl} G(k, l) - 1, \end{aligned} \quad (\text{B2})$$

where

$$G(k, l) = \phi(\beta[C(k, l) + \lambda(k) + \mu(l) + x]) \quad (\text{B3})$$

and

$$\phi(t) = \frac{e^{-t}}{e^{-t} - 1} + \frac{1}{t}. \quad (\text{B4})$$

Let ϕ' be the derivative of the function ϕ , i.e.,

$$\phi'(t) = \frac{e^{-t}}{(e^{-t} - 1)^2} - \frac{1}{t^2}. \quad (\text{B5})$$

We note first that $\phi'(t) \in [-\frac{1}{12}, 0) \quad \forall x \in \mathbb{R}$, i.e., that $\phi'(t)$ is always strictly negative. We define the matrix G' such that

$$G'(k, l) = \phi'(\beta[C(k, l) + \lambda(k) + \mu(l) + x]). \quad (\text{B6})$$

From the expression of the first derivatives, we obtain

$$\begin{aligned} H(k, i) &= \frac{\partial^2 F_\beta(\boldsymbol{\lambda}, \boldsymbol{\mu}, x)}{\partial \lambda(k) \partial \lambda(i)} = \beta \delta_{ki} \sum_l G'(k, l) - \frac{\delta_{ki}}{2\alpha_1(k)}, \\ H(k, l) &= \frac{\partial^2 F_\beta(\boldsymbol{\lambda}, \boldsymbol{\mu}, x)}{\partial \lambda(k) \partial \mu(l)} = \beta G'(k, l), \\ H(k, x) &= \frac{\partial^2 F_\beta(\boldsymbol{\lambda}, \boldsymbol{\mu}, x)}{\partial \lambda(k) \partial x} = \beta \sum_l G'(k, l), \\ H(l, m) &= \frac{\partial^2 F_\beta(\boldsymbol{\lambda}, \boldsymbol{\mu}, x)}{\partial \mu(l) \partial \mu(m)} = \beta \delta_{lm} \sum_k G'(k, l) - \frac{\delta_{lm}}{2\alpha_2(l)}, \\ H(l, x) &= \frac{\partial^2 F_\beta(\boldsymbol{\lambda}, \boldsymbol{\mu}, x)}{\partial \mu(l) \partial x} = \beta \sum_k G'(k, l), \\ H(x, x) &= \frac{\partial^2 F_\beta(\boldsymbol{\lambda}, \boldsymbol{\mu}, x)}{\partial x \partial x} = \beta \sum_{kl} G'(k, l), \end{aligned}$$

where δ are Kronecker functions, the indices k and i belong to $[1, N_1]$, the indices l and m belong to $[1, N_2]$, and index x refers to variable x .

Let $\mathbf{x} = (\mathbf{x}_1, \mathbf{x}_2, x_3)$ be an arbitrary nonzero vector of size $N_1 + N_2 + 1$. The quadratic form $Q(\mathbf{x}) = \mathbf{x}^T H \mathbf{x}$ is equal to

$$\begin{aligned} Q(\mathbf{x}) &= \sum_{i,k} x_1(k)H(k, i)x_1(i) + 2 \sum_{k,l} x_1(k)H(k, l)x_2(l) \\ &+ 2 \sum_k x_1(k)H(k, x)x_3 + \sum_{l,m} x_2(l)H(l, m)x_2(m) \\ &+ 2 \sum_l x_2(l)H(l, x)x_3 + H(x, x)x_3^2. \end{aligned}$$

Replacing with the expressions of the second derivatives above, we get

$$\begin{aligned} Q(\mathbf{x}) &= \beta \sum_{k,l} x_1(k)^2 G'(k, l) + \beta \sum_{k,l} x_2(l)^2 G'(k, l) \\ &+ \beta x_3^2 \sum_{k,l} G'(k, l) + 2\beta \sum_{k,l} x_1(k)G'(k, l)x_2(l) \\ &+ 2\beta \sum_{k,l} x_1(k)G'(k, l)x_3 + 2\beta \sum_{k,l} x_2(l)G'(k, l)x_3 \\ &- \frac{1}{2} \sum_k \frac{x_1(k)^2}{\alpha_1(k)} - \frac{1}{2\alpha_2} \sum_l \frac{x_2(l)^2}{\alpha_2(l)}. \end{aligned}$$

After factorization,

$$\begin{aligned} Q(\mathbf{x}) &= \beta \sum_{k,l} [x_1(k) + x_2(l) + x_3]^2 G'(k, l) \\ &- \frac{1}{2} \sum_k \frac{x_1(k)^2}{\alpha_1(k)} - \frac{1}{2} \sum_l \frac{x_2(l)^2}{\alpha_2(l)}. \end{aligned} \quad (\text{B7})$$

As $G'(k, l)$ is based on the function ϕ' that is strictly negative, the summands after the factor β in the equation above are negative for all k and l . In addition, as $\alpha_1(k) > 0$ and $\alpha_2(l) > 0$, the second and third terms are also negative. These two terms are zero if and only if $\forall k x_1(k) = 0$ and $\forall l x_2(l) = 0$. In this case,

$$Q(\mathbf{x}) = \beta x_3 \sum_{k,l} G'(k, l).$$

As the $G'(k, l)$ are nonzero [as $\phi'(x)$ is nonzero], and as x_3 is not zero (otherwise \mathbf{x} would be zero), $Q(\mathbf{x})$ is strictly negative for all nonzero vectors \mathbf{x} . The Hessian H is therefore negative-definite. As a consequence, $F_\beta(\boldsymbol{\lambda}, \boldsymbol{\mu}, x)$ is strictly concave.

APPENDIX C: PROOF OF PROPOSITION 2: RETRIEVING THE TRANSPORT PLAN AND MASSES FROM THE SPA SOLUTIONS

Let us first recall the definition of the partition function [Eq. (28)]

$$\begin{aligned} Z &= \int_0^1 \prod_{kl} dG(k, l) \int_{-\infty}^{+\infty} \prod_k dm_1(k) \int_{-\infty}^{+\infty} \prod_l dm_2(l) \\ &\times e^{-\beta(\sum_{kl} C(k,l)G(k,l) + \sum_k \alpha_1(k)m_1^2(k) + \sum_l \alpha_2(l)m_2^2(l))} \end{aligned}$$

$$\begin{aligned} &\times \prod_k \delta\left(\sum_l G(k, l) - m_1(k)\right) \\ &\times \prod_l \delta\left(\sum_k G(k, l) - m_2(l)\right) \\ &\times \prod_{kl} \delta\left(\sum_{kl} G(k, l) - 1\right) \end{aligned}$$

and of the corresponding effective free energy [Eq. (31)]

$$\begin{aligned} F_\beta &= -\left(x + \frac{1}{4} \sum_k \frac{\lambda^2(k)}{\alpha_1(k)} + \frac{1}{4} \sum_l \frac{\mu^2(l)}{\alpha_2(l)}\right) \\ &- \frac{1}{\beta} \sum_{kl} \ln \left[\frac{1 - e^{-\beta[C(k,l) + \lambda(k) + \mu(l) + x]}}{\beta[C(k, l) + \lambda(k) + \mu(l) + x]} \right]. \end{aligned}$$

F_β is a function of $N_1 + N_2 + 1$ variables, namely $\lambda(k)$ for $k \in [1, N_1]$, $\mu(l)$ for $l \in [1, N_2]$, and x . We have proved in Appendix B that F_β is strictly concave and has therefore a unique optimum. The values of $\boldsymbol{\lambda}$, $\boldsymbol{\mu}$, and x at this optimum are referred to as $\boldsymbol{\lambda}^{\text{MF}}$, $\boldsymbol{\mu}^{\text{MF}}$, and x^{MF} , respectively.

The transport plan G . The expected value for the transport between point k in S_1 and point l in S_2 is given by

$$\bar{G}(k, l) = \frac{1}{\beta} \frac{\partial \ln(Z)}{\partial C(k, l)} = -\frac{\partial F_\beta}{\partial C(k, l)}(\boldsymbol{\lambda}^{\text{MF}}, \boldsymbol{\mu}^{\text{MF}}, x^{\text{MF}}).$$

Using the expression for the free energy, we get

$$\bar{G}(k, l) = \phi(\beta[C(k, l) + \lambda(k)^{\text{MF}} + \mu(l)^{\text{MF}} + x^{\text{MF}}]),$$

i.e., the value found as a solution of the SPA system does give us the expected transport plan between the two sets of points.

The masses \mathbf{m}_1 and \mathbf{m}_2 . To find the expected values $\bar{\mathbf{m}}_1$ and $\bar{\mathbf{m}}_2$ for the masses associated with the points in S_1 and S_2 , we need to introduce two vector fields \mathbf{u}_1 and \mathbf{u}_2 , and modify the partition function:

$$\begin{aligned} Z(\mathbf{u}_1, \mathbf{u}_2) &= \int_0^1 \prod_{kl} dG(k, l) \int_{-\infty}^{+\infty} \prod_k dm_1(k) \int_{-\infty}^{+\infty} \prod_l dm_2(l) \\ &\times e^{-\beta(\sum_{kl} C(k,l)G(k,l) + \sum_k \alpha_1(k)m_1^2(k) + \sum_l \alpha_2(l)m_2^2(l))} \\ &\times e^{\beta(\sum_k u_1(k)m_1(k) + \sum_l u_2(l)m_2(l))} \\ &\times \prod_k \delta\left(\sum_l G(k, l) - m_1(k)\right) \\ &\times \prod_l \delta\left(\sum_k G(k, l) - m_2(l)\right) \\ &\times \prod_{kl} \delta\left(\sum_{kl} G(k, l) - 1\right). \end{aligned}$$

Following the same procedure as described in the main text for evaluating this modified partition function, we find

$$\begin{aligned} F_\beta(\mathbf{u}_1, \mathbf{u}_2, \boldsymbol{\lambda}, \boldsymbol{\mu}, x) &= -x - \frac{1}{4} \sum_k \frac{[\lambda(k) + u_1(k)]^2}{\alpha_1(k)} \\ &\quad - \frac{1}{4} \sum_l \frac{[\mu(l) + u_2(l)]^2}{\alpha_2(l)} \\ &\quad - \frac{1}{\beta} \sum_{kl} \ln \left[\frac{1 - e^{-\beta[C(k,l) + \lambda(k) + \mu(l) + x]}}{\beta[C(k,l) + \lambda(k) + \mu(l) + x]} \right]. \end{aligned}$$

Then, the expected value for the mass $m_1(k)$ of point k in S_1 is given by

$$\bar{m}_1(k) = - \left. \frac{\partial F_\beta}{\partial u_1(k)} \right|_{\mathbf{u}_1=0, \mathbf{u}_2=0, \boldsymbol{\lambda}=\boldsymbol{\lambda}^{\text{MF}}, \boldsymbol{\mu}=\boldsymbol{\mu}^{\text{MF}}, x=x^{\text{MF}}},$$

i.e.,

$$\bar{m}_1(k) = \frac{\lambda(k)^{\text{MF}}}{2\alpha_1(k)}$$

and similarly,

$$\begin{aligned} \bar{m}_2(k) &= - \left. \frac{\partial F_\beta}{\partial u_2(k)} \right|_{\mathbf{u}_1=0, \mathbf{u}_2=0, \boldsymbol{\lambda}=\boldsymbol{\lambda}^{\text{MF}}, \boldsymbol{\mu}=\boldsymbol{\mu}^{\text{MF}}, x=x^{\text{MF}}} \\ &= \frac{\mu(l)^{\text{MF}}}{2\alpha_2(l)}. \end{aligned}$$

APPENDIX D: PROOF OF PROPOSITION 3: MONOTONICITY AND LIMITS OF $F^{\text{MF}}(\beta)$

Let us consider two sets of points S_1 and S_2 in a metric space \mathcal{M} with associated variable-mass vectors \mathbf{m}_1 and \mathbf{m}_2 , respectively. We associate this system with a cost matrix C and a transport polytope $\mathcal{S}(S_1, S_2)$. In Appendix B we established that the exact free energy and internal energy defined in Eqs. (23) and (24), respectively, are monotonic functions of the parameter β , and converge to the actual optimal transport distance $d(S_1, S_2)$ when $\beta \rightarrow \infty$. Here we consider the approximation of those quantities obtained with the saddle point approximation, namely the mean-field values F^{MF} and U^{MF} , and we show that they satisfy the same properties.

The effective free energy $F_\beta = F_\beta(\boldsymbol{\lambda}, \boldsymbol{\mu}, x)$ defined in Eq. (31) is a function of the cost matrix C and of real unconstrained variables λ_k , μ_l , and x . For the sake of simplicity, for any $(k, l) \in [1, N_1] \times [1, N_2]$, we define

$$x_{kl} = C(k, l) + \lambda(k) + \mu(l) + x. \quad (\text{D1})$$

The effective free energy is then

$$\begin{aligned} F_\beta &= - \left(x + \frac{1}{4} \sum_k \frac{\lambda^2(k)}{\alpha_1(k)} + \frac{1}{4} \sum_l \frac{\mu^2(l)}{\alpha_2(l)} \right) \\ &\quad - \frac{1}{\beta} \sum_{kl} \ln \left(\frac{1 - e^{-\beta x_{kl}}}{\beta x_{kl}} \right). \end{aligned} \quad (\text{D2})$$

As written above, F_β is a function of the independent variables β , $\lambda(k)$, $\mu(l)$, and x . However, under the saddle point

approximation, the variables $\lambda(k)$, $\mu(l)$, and x are constrained by the conditions

$$\frac{\partial F_\beta}{\partial \lambda(k)} = 0, \quad \frac{\partial F_\beta}{\partial \mu(l)} = 0, \quad \frac{\partial F_\beta}{\partial x} = 0. \quad (\text{D3})$$

We write $\boldsymbol{\lambda}^{\text{MF}}$, $\boldsymbol{\mu}^{\text{MF}}$, and x^{MF} for the values that satisfy those constraints. The corresponding free energy is written as $F^{\text{MF}}(\beta) = F_\beta(\boldsymbol{\lambda}^{\text{MF}}, \boldsymbol{\mu}^{\text{MF}}, x^{\text{MF}})$. In the following, we will use the notations $\frac{dF^{\text{MF}}(\beta)}{d\beta}$ and $\frac{\partial F^{\text{MF}}(\beta)}{\partial \beta}$ to differentiate between the total derivative and partial derivative of $F^{\text{MF}}(\beta)$ with respect to β , respectively. Based on the chain rule,

$$\begin{aligned} \frac{dF^{\text{MF}}(\beta)}{d\beta} &= \frac{\partial F_\beta}{\partial \beta} + \sum_k \frac{\partial F_\beta}{\partial \lambda(k)} \frac{\partial \lambda(k)}{\partial \beta} \\ &\quad + \sum_l \frac{\partial F_\beta}{\partial \mu(l)} \frac{\partial \mu(l)}{\partial \beta} + \frac{\partial F_\beta}{\partial x} \frac{\partial x}{\partial \beta}, \end{aligned} \quad (\text{D4})$$

where the derivatives are computed at $(\boldsymbol{\lambda}^{\text{MF}}, \boldsymbol{\mu}^{\text{MF}}, x^{\text{MF}})$. Therefore,

$$\frac{dF^{\text{MF}}(\beta)}{d\beta} = \frac{\partial F_\beta}{\partial \beta}, \quad (\text{D5})$$

namely that the total derivative with respect to β is in this specific case equal to the corresponding partial derivative, which is easily computed to be

$$\frac{dF^{\text{MF}}(\beta)}{d\beta} = \frac{1}{\beta^2} \sum_{kl} \left[\ln \left(\frac{1 - e^{-\beta x_{kl}^{\text{MF}}}}{\beta x_{kl}^{\text{MF}}} \right) + \beta x_{kl}^{\text{MF}} \phi(\beta x_{kl}^{\text{MF}}) \right], \quad (\text{D6})$$

where $\phi(t) = \frac{e^{-t}}{e^{-t}-1} + \frac{1}{t}$. Let $f(t) = \ln \left(\frac{1-e^{-t}}{t} \right) + t\phi(t)$. $\phi(x)$ is monotonically constrained in the interval $[0, 1]$ and therefore correctly represents the possible values for the corresponding transport plan. The function $f(t)$ is continuous and defined over all real values t [with the extension $f(0) = 0$] and is bounded above by 0, i.e., $f(t) \leq 0 \quad \forall t \in \mathbb{R}$.

As

$$\frac{dF^{\text{MF}}(\beta)}{d\beta} = \frac{1}{\beta^2} \sum_{kl} f(\beta x_{kl}^{\text{MF}}) \quad (\text{D7})$$

we conclude that

$$\frac{dF^{\text{MF}}(\beta)}{d\beta} \leq 0, \quad (\text{D8})$$

namely that $F^{\text{MF}}(\beta)$ is a monotonically decreasing function of β . In addition, we note that $F^{\text{MF}}(\beta)$ is the mean-field approximation of the true free energy \mathcal{F}_β and that this approximation becomes exact when β tends to ∞ . Therefore,

$$\lim_{\beta \rightarrow \infty} F^{\text{MF}}(\beta) = \lim_{\beta \rightarrow \infty} \mathcal{F}(\beta) = d_u(S_1, S_2), \quad (\text{D9})$$

where $d_u(S_1, S_2)$ is the variable-mass optimal-transport cost between the two sets of points S_1 and S_2 .

**APPENDIX E: PROOF OF PROPOSITION 3:
MONOTONICITY AND LIMITS OF $U^{\text{MF}}(\beta)$**

Let

$$U_\beta = \sum_{kl} C_{kl} G(k, l) + \sum_k \alpha_1(k) m_1^2(k) + \sum_l \alpha_2(l) m_2^2(l) \quad (\text{E1})$$

and the corresponding mean-field approximation of the internal energy at the saddle point,

$$U^{\text{MF}}(\beta) = U_\beta(\lambda^{\text{MF}}, \mu^{\text{MF}}, x^{\text{MF}}). \quad (\text{E2})$$

Before computing $\frac{dU^{\text{MF}}(\beta)}{d\beta}$, let us prove the following property:
Property 4.

$$\begin{aligned} U^{\text{MF}}(\beta) &= F^{\text{MF}}(\beta) + \beta \frac{dF^{\text{MF}}(\beta)}{d\beta} \\ &= \frac{d[\beta F^{\text{MF}}(\beta)]}{d\beta}, \end{aligned} \quad (\text{E3})$$

i.e., it extends the relationship (A4) known between the free energy and the average energy to their mean-field counterparts.

Proof. Let us recall that

$$x_{kl}^{\text{MF}} = C(k, l) + \lambda^{\text{MF}}(k) + \mu^{\text{MF}}(l) + x^{\text{MF}}.$$

All mean-field values correspond to the minimum of the effective free energy, for which the constraints are satisfied, namely

$$\begin{aligned} G^{\text{MF}}(k, l) &= \phi(\beta x_{kl}^{\text{MF}}), \\ \sum_l G^{\text{MF}}(k, l) &= \frac{\lambda^{\text{MF}}(k)}{2\alpha_1(k)} = m_1^{\text{MF}}(k), \\ \sum_k G^{\text{MF}}(k, l) &= \frac{\mu^{\text{MF}}(l)}{2\alpha_2(l)} = m_2^{\text{MF}}(l), \\ \sum_{kl} G^{\text{MF}}(k, l) &= 1. \end{aligned}$$

Therefore,

$$\begin{aligned} \sum_{kl} x_{kl}^{\text{MF}} \phi(x_{kl}^{\text{MF}}) &= \sum_{kl} C(k, l) G^{\text{MF}}(k, l) \\ &+ \sum_k \lambda^{\text{MF}}(k) \sum_l G^{\text{MF}}(k, l) \\ &+ \sum_l \mu^{\text{MF}}(l) \sum_k G^{\text{MF}}(k, l) \\ &+ x \sum_{kl} G^{\text{MF}}(k, l), \end{aligned}$$

i.e.,

$$\begin{aligned} \sum_{kl} x_{kl}^{\text{MF}} \phi(x_{kl}^{\text{MF}}) &= \sum_{kl} C(k, l) G^{\text{MF}}(k, l) \\ &+ \frac{1}{2} \sum_k \frac{[\lambda^{\text{MF}}(k)]^2}{\alpha_1(k)} \\ &+ \frac{1}{2} \sum_l \frac{[\mu^{\text{MF}}(l)]^2}{\alpha_2(l)} + x. \end{aligned}$$

Let us now rewrite Eq. (D6) as

$$\begin{aligned} \beta \frac{dF^{\text{MF}}(\beta)}{d\beta} &= -F^{\text{MF}}(\beta) - x - \frac{1}{4} \sum_k \frac{[\lambda^{\text{MF}}(k)]^2}{\alpha_1(k)} \\ &- \frac{1}{4} \sum_l \frac{[\mu^{\text{MF}}(l)]^2}{\alpha_2(l)} + \sum_{kl} x_{kl}^{\text{MF}} \phi(x_{kl}^{\text{MF}}). \end{aligned}$$

We get

$$\begin{aligned} \beta \frac{dF^{\text{MF}}(\beta)}{d\beta} &= -F^{\text{MF}}(\beta) + \sum_{kl} C(k, l) G^{\text{MF}}(k, l) \\ &+ \frac{1}{4} \sum_k \frac{[\lambda^{\text{MF}}(k)]^2}{\alpha_1(k)} + \frac{1}{4} \sum_l \frac{[\mu^{\text{MF}}(l)]^2}{\alpha_2(l)} \\ &= -F^{\text{MF}}(\beta) + \sum_{kl} C(k, l) G^{\text{MF}}(k, l) \\ &+ \sum_k \alpha_1(k) [m_1^{\text{MF}}(k)]^2 + \sum_l \alpha_2(l) [m_2^{\text{MF}}(l)]^2, \end{aligned}$$

i.e.,

$$\beta \frac{dF^{\text{MF}}(\beta)}{d\beta} = -F^{\text{MF}}(\beta) + U^{\text{MF}}(\beta),$$

which concludes the proof.

Based on the chain rule,

$$\begin{aligned} \frac{dU^{\text{MF}}(\beta)}{d\beta} &= \frac{\partial U^{\text{MF}}(\beta)}{\partial \beta} + \sum_k \frac{\partial U^{\text{MF}}(\beta)}{\partial \lambda(k)} \frac{\partial \lambda(k)}{\partial \beta} \\ &+ \sum_l \frac{\partial U^{\text{MF}}(\beta)}{\partial \mu(l)} \frac{\partial \mu(l)}{\partial \beta} + \frac{\partial U^{\text{MF}}(\beta)}{\partial x} \frac{\partial x}{\partial \beta}. \end{aligned} \quad (\text{E4})$$

Let us compute all partial derivatives in this equation using proposition 4,

$$\begin{aligned} \frac{\partial U^{\text{MF}}(\beta)}{\partial \lambda(k)} &= \frac{\partial F^{\text{MF}}(\beta)}{\partial \lambda(k)} + \beta \frac{\partial}{\partial \lambda(k)} \left(\frac{\partial F^{\text{MF}}(\beta)}{\partial \beta} \right) \\ &= \frac{\partial F^{\text{MF}}(\beta)}{\partial \lambda(k)} + \beta \frac{\partial}{\partial \beta} \left(\frac{\partial F^{\text{MF}}(\beta)}{\partial \lambda(k)} \right) \\ &= 0, \end{aligned} \quad (\text{E5})$$

where the zero is a consequence of the SPA constraints. Similarly, we find

$$\frac{\partial U^{\text{MF}}(\beta)}{\partial \mu(l)} = 0, \quad \frac{\partial U^{\text{MF}}(\beta)}{\partial x} = 0. \quad (\text{E6})$$

Finally,

$$\begin{aligned} \frac{\partial U^{\text{MF}}(\beta)}{\partial \beta} &= 2 \frac{\partial F^{\text{MF}}(\beta)}{\partial \beta} + \beta \frac{\partial}{\partial \beta} \left(\frac{\partial F^{\text{MF}}(\beta)}{\partial \beta} \right) \\ &= 2 \frac{\partial F^{\text{MF}}(\beta)}{\partial \beta} \\ &+ \beta \left(-\frac{2}{\beta} \frac{\partial F^{\text{MF}}(\beta)}{\partial \beta} + \frac{1}{\beta^2} \sum_{kl} x_{kl}^{\text{MF}} f'(\beta x_{kl}^{\text{MF}}) \right), \end{aligned}$$

i.e.,

$$\frac{\partial U^{\text{MF}}(\beta)}{\partial \beta} = \frac{1}{\beta} \sum_{kl} x_{kl}^{\text{MF}} f'(\beta x_{kl}^{\text{MF}}),$$

where f is defined above. As $f'(t) = t\phi'(t)$, we get

$$\frac{\partial U^{\text{MF}}(\beta)}{\partial \beta} = \frac{1}{\beta} \sum_{kl} (x_{kl}^{\text{MF}})^2 \phi'(\beta x_{kl}^{\text{MF}}). \quad (\text{E7})$$

As $(x_{kl}^{\text{MF}})^2$ is always positive, and $\phi'(x)$ is always negative, we have

$$\frac{dU^{\text{MF}}(\beta)}{d\beta} = \frac{\partial U^{\text{MF}}(\beta)}{\partial \beta} \leq 0 \quad (\text{E8})$$

and the function $U^{\text{MF}}(\beta)$ is a monotonically decreasing function of β . In addition, we note that $U^{\text{MF}}(\beta)$ is the mean-field approximation of the true internal energy E_β and that this approximation becomes exact when β tends to ∞ . Therefore,

$$\lim_{\beta \rightarrow \infty} U^{\text{MF}}(\beta) = \lim_{\beta \rightarrow \infty} E_\beta = d_u(S_1, S_2), \quad (\text{E9})$$

where $d_u(S_1, S_2)$ is the variable-mass optimal-transport cost between the two sets of points S_1 and S_2 .

APPENDIX F: EFFICIENT FORMULATION OF THE JACOBIAN SYSTEM FOR SOLVING THE SPA EQUATIONS

The saddle point Eqs. (33) form a nonlinear system of $N_1 + N_2 + 1$ equations, and the same number of variables. We rewrite this system as

$$\mathbf{A}_\lambda = \mathbf{0}, \quad \mathbf{A}_\mu = \mathbf{0}, \quad A_x = 0,$$

where $\mathbf{A} = (\mathbf{A}_\lambda, \mathbf{A}_\mu, A_x)$ is a vector of predicates defined as

$$A_\lambda(k) = - \sum_l \frac{e^{-\beta x_{kl}}}{e^{-\beta x_{kl}} - 1} - \sum_l \frac{1}{\beta x_{kl}} + \frac{\lambda(k)}{2\alpha_1(k)},$$

$$A_\mu(l) = - \sum_k \frac{e^{-\beta x_{kl}}}{e^{-\beta x_{kl}} - 1} - \sum_k \frac{1}{\beta x_{kl}} + \frac{\mu(l)}{2\alpha_2(l)},$$

$$A_x = - \sum_{kl} \frac{e^{-\beta x_{kl}}}{e^{-\beta x_{kl}} - 1} - \sum_{kl} \frac{1}{\beta x_{kl}} + 1,$$

where $x_{kl} = C(k, l) + \lambda(k) + \mu(l) + x$. It is solved using an iterative Newton-Raphson method as follows. Let us assume that we know an initial solution $\mathbf{X}_0 = (\lambda_0, \mu_0, x)$ for this system. Taylor expansions of the predicates \mathbf{A} in the neighborhood of this solution lead to the following system of equations:

$$J(\mathbf{X}_0)\delta\mathbf{X} = -\mathbf{A}(\mathbf{X}_0), \quad (\text{F1})$$

where $\delta\mathbf{X} = (\delta\lambda, \delta\mu, \delta x)$ is the correction to be applied to \mathbf{X}_0 , $\mathbf{A}(\mathbf{X}_0)$ is the vector of values of the $N_1 + N_2 + 1$ predicates at \mathbf{X}_0 , and $J(\mathbf{X}_0)$ is the Jacobian of \mathbf{A} taken at \mathbf{X}_0 . We note that this Jacobian J is equal to the opposite of the Hessian of the free-energy function F . As this free energy is concave, the Jacobian is then positive-definite. It can be written in block form:

$$J(\mathbf{X}_0) = \begin{bmatrix} D_\lambda & G' & \mathbf{v}_\lambda \\ G'^T & D_\mu & \mathbf{v}_\mu \\ \mathbf{v}_\lambda^T & \mathbf{v}_\mu^T & d_x \end{bmatrix},$$

where $G'(k, l) = \beta\phi'(\beta x_{kl})$, \mathbf{v}_λ is a vector of size N_1 such that $v_\lambda(k) = \sum_l G'(k, l)$, \mathbf{v}_μ is a vector of size N_2 such that $v_\mu(l) = \sum_k G'(k, l)$, D_λ is the diagonal matrix defined by $D_\lambda(k, k) = v_\lambda(k) - \frac{1}{2\alpha_1(k)}$, D_μ is the diagonal matrix defined by $D_\mu(l, l) = v_\mu(l) - \frac{1}{2\alpha_2(l)}$, $d_x = \sum_{kl} G'(k, l)$, and $\phi'(x)$ is the derivative of the function $\phi(x)$. The system of equations (F1) can then be rewritten as

$$\begin{bmatrix} D_\lambda & G' & \mathbf{v}_\lambda \\ G'^T & D_\mu & \mathbf{v}_\mu \\ \mathbf{v}_\lambda^T & \mathbf{v}_\mu^T & d_x \end{bmatrix} \begin{bmatrix} \lambda \\ \mu \\ x \end{bmatrix} = - \begin{bmatrix} \mathbf{A}_\lambda \\ \mathbf{A}_\mu \\ A_x \end{bmatrix}$$

or equivalently as

$$D_\lambda \lambda + G' \mu + x \mathbf{v}_\lambda = -\mathbf{A}_\lambda, \quad (\text{F2a})$$

$$G'^T \lambda + D_\mu \mu + x \mathbf{v}_\mu = -\mathbf{A}_\mu, \quad (\text{F2b})$$

$$\langle \mathbf{v}_\lambda, \lambda \rangle + \langle \mathbf{v}_\mu, \mu \rangle + x d_x = -A_x, \quad (\text{F2c})$$

where $\langle \cdot, \cdot \rangle$ is the inner product. From Eq. (F2c), which is in fact scalar, we get

$$x = -\frac{1}{d_x} (A_x + \langle \mathbf{v}_\lambda, \lambda \rangle + \langle \mathbf{v}_\mu, \mu \rangle). \quad (\text{F3})$$

[Note that since d_x is the sum of strictly negative numbers, as $\phi'(x) < 0$, it is strictly negative.] Replacing in (F2a) and (F2b), we get a new system of $N_1 + N_2$ equations:

$$E_\lambda \lambda + H \mu = \mathbf{B}_\lambda, \quad (\text{F4a})$$

$$H^T \lambda + E_\mu \mu = \mathbf{B}_\mu, \quad (\text{F4b})$$

where

$$E_\lambda = D_\lambda - \mathbf{v}_\lambda \mathbf{v}_\lambda^T,$$

$$E_\mu = D_\mu - \mathbf{v}_\mu \mathbf{v}_\mu^T,$$

$$H = G' - \mathbf{v}_\lambda \mathbf{v}_\mu^T$$

for the left side of the equations, and

$$\mathbf{B}_\lambda = -\mathbf{A}_\lambda + \frac{A_x}{d_x} \mathbf{v}_\lambda, \quad (\text{F5})$$

$$\mathbf{B}_\mu = -\mathbf{A}_\mu + \frac{A_x}{d_x} \mathbf{v}_\mu \quad (\text{F6})$$

for the right side. We solve this system with a preconditioned conjugate-gradient approach. We found that an efficient precondition M is based on an incomplete LDU factorization:

$$M = \begin{bmatrix} I_{N_1} & 0 \\ H E_\lambda^{-1} & I_{N_2} \end{bmatrix} \begin{bmatrix} E_\lambda & 0 \\ 0 & E_\mu \end{bmatrix} \begin{bmatrix} I_{N_1} & E_\lambda^{-1} H \\ 0 & I_{N_2} \end{bmatrix},$$

where I_{N_1} and I_{N_2} are identity matrices of size N_1 and N_2 . Note that this precondition requires the inverse of the matrix E_λ . This inverse is easy to compute, as E_λ is a one-rank update of

the diagonal matrix D_λ . Therefore,

$$E_\lambda^{-1} = D_\lambda^{-1} + a\mathbf{w}\mathbf{w}^T$$

with $\mathbf{w} = D_\lambda^{-1}\mathbf{v}_\lambda$ and $a = 1/(d_x - (\mathbf{w}, \mathbf{v}_\lambda))$. Once the system of Eqs. (F4) has been solved for λ and μ , x is derived from Eq. (F3).

-
- [1] G. Monge, *Hist. Acad. R. Sci. Mém. Math. Phys. Acad.* **1784**, 666 (1781).
- [2] C. Villani, *Topics in Optimal Transportation* (American Mathematical Society, Providence, RI, 2003).
- [3] L. Ning, F. Carli, A. Ebtehaj, E. Foufoula-Georgiou, and T. Georgiou, *Water Resour. Res.* **50**, 5817 (2014).
- [4] L. Ning, T. Georgiou, and A. Tannenbaum, *IEEE Trans. Autom. Control* **60**, 373 (2015).
- [5] A. Halder and E. Wendel, in *Proceedings of the 2016 American Control Conference* (2016), pp. 7249–7254.
- [6] Y. Chen, E. Haber, K. Yamamoto, T. Georgiou, and A. Tannenbaum, *J. Sci. Comput.* **77**, 79 (2018).
- [7] J. Solomon, R. Rustamov, and L. Guibas, in *Proceedings of the 31st International Conference on Machine Learning* (2014), pp. 306–314.
- [8] C. Frogner, C. Zhang, H. Mobahi, M. Araya-Polo, and T. Poggio, in *Proceedings of the 28th Advances in Neural Information Processing Systems (NIPS)* (2015), pp. 2053–2061.
- [9] S. Kolouri, S. R. Park, M. Thorpe, D. Slepcev, and G. K. Rohde, *IEEE Sign. Proc. Mag.* **34**, 43 (2017).
- [10] Y. Rubner, C. Tomasi, and L. Guibas, in *Proceedings of the Sixth International Conference on Computer Vision* (1998), pp. 59–66.
- [11] Y. Rubner, C. Tomasi, and L. Guibas, *Int. J. Comput. Vision* **40**, 99 (2000).
- [12] S. Haker, L. Zhu, A. Tannenbaum, and S. Angenent, *Int. J. Comput. Vision* **60**, 225 (2004).
- [13] L.-P. Saumier, M. Agueh, and B. Khouider, [arXiv:1009.6039](https://arxiv.org/abs/1009.6039) [math.NA].
- [14] S. Kolouri, A. Tosun, J. Ozolek, and G. Rohde, *Pattern Recog.* **51**, 453 (2016).
- [15] J. Lee, N. Bertrand, and C. Rozell, [arXiv:1909.00149](https://arxiv.org/abs/1909.00149) [eess.IV].
- [16] G. Huang, C. Guo, M. Kusner, Y. Sun, F. Sha, and K. Weinberger, in *Advances in Neural Information Processing Systems* (2016), pp. 4862–4870.
- [17] A. Rolet, M. Cuturi, and G. Peyré, in *Proceedings of the 19th International Conference on Artificial Intelligence and Statistics* (2016), pp. 630–638.
- [18] N. Guillen and R. McCaen, [arXiv:1011.2911](https://arxiv.org/abs/1011.2911) [math.DG].
- [19] A. Figalli and C. Villani, *Optimal transport and curvature, in Nonlinear PDE's and Applications* (Springer, Berlin, 2011), pp. 171–217.
- [20] Z. Su, Y. Wang, R. Shi, W. Zeng, J. Sun, F. Luo, and X. Gu, *IEEE Trans. Pattern Anal. Mach. Intell.* **37**, 2246 (2015).
- [21] M. Ma, N. Lei, W. Chen, K. Su, and X. Gu, *Graph. Mod.* **90**, 13 (2017).
- [22] Y. Chen, T. Georgiou, M. Pavon, and A. Tannenbaum, *IEEE Trans. Autom. Contr.* **62**, 4675 (2017).
- [23] C.-C. Ni, Y.-Y. Lin, F. Luo, and J. Gao, *Sci. Rep.* **9**, 9984 (2019).
- [24] Y. Chen, T. T. Georgiou, M. Pavon, and A. Tannenbaum, *IEEE Trans. Control. Netw. Syst.* **7**, 923 (2020).
- [25] G. Schiebinger, J. Shu, M. Tabaka, B. Cleary, V. Subramanian, A. Solomon, J. Gould, S. Liu, S. Lin, P. Berube, L. Lee, J. Chen, J. Brumbaugh, P. Rigollet, K. Hochedlinger, R. Jaenisch, A. Regev, and E. Lander, *Cell* **176**, 928 (2019).
- [26] P. Dixit and K. Dill, *J. Chem. Phys.* **150**, 054105 (2019).
- [27] Y. Chen, T. T. Georgiou, and A. Tannenbaum, *IEEE Trans. Autom. Control* **63**, 2612 (2018).
- [28] Y. Chen, T. Georgiou, and A. Tannenbaum, *SIAM J. Appl. Math.* **8**, 1682 (2018).
- [29] C. Villani, *Optimal Transport: Old and New*, Grundlehren der Mathematischen Wissenschaften (Springer, Berlin, 2008).
- [30] F. Santambrogio, *Optimal Transport for Applied Mathematicians*, Progress in Nonlinear Differential Equations and their Applications (Springer, Berlin, 2015).
- [31] B. Levy and E. Schwindt, *Comput. Graph.* **72**, 135 (2018).
- [32] G. Peyré and M. Cuturi, *Found. Trends Mach. Learn.* **11**, 355 (2019).
- [33] A. Figalli, *Arch. Ration. Mech. Anal.* **195**, 533 (2010).
- [34] L. Evans and W. Gangbo, *Differential Equations Methods for the Monge-Kantorovich Mass Transfer Problem*, Mem. Am. Math. Soc. (American Mathematical Society, Providence, RI, 1999), Vol. 137.
- [35] G. Bouchitté and G. Buttazzo, *J. Eur. Math. Soc.* **3**, 139 (2001).
- [36] J. Benamou and Y. Brenier, *Numer. Math.* **84**, 375 (2000).
- [37] Y. Brenier, in *Optimal Transportation and Applications* (Springer, Heidelberg, 2003), pp. 91–121.
- [38] H. Lavenant, S. Claici, E. Chien, and J. Solomon, *ACM Trans. Graph.* **37**, 250:1 (2018).
- [39] L. Cafferelli and R. McCann, *Ann. Math.* **171**, 673 (2010).
- [40] T. Georgiou, J. Karlsson, and S. Takyar, *IEEE Trans. Signal Proc.* **57**, 859 (2009).
- [41] B. Piccoli and F. Rossi, [arXiv:1304.7014](https://arxiv.org/abs/1304.7014) [math.AP].
- [42] B. Piccoli and F. Rossi, *Arch. Ration. Mech. Anal.* **211**, 335 (2014).
- [43] M. Liero and A. M. ans G. Savaré, *SIAM J. Math. Anal.* **48**, 2869 (2016).
- [44] L. Chizat, G. Peyré, B. Schmitzer, and F.-X. Vialard, *J. Funct. Anal.* **274**, 3090 (2018).
- [45] L. Chizat, G. Peyré, B. Schmitzer, and F.-X. Vialard, *Found. Comput. Math.* **18**, 1 (2018).
- [46] T. Séjourné, J. Freydy, F.-X. Vialard, A. Trouvé, and G. Peyré, [arXiv:1910.12958](https://arxiv.org/abs/1910.12958) [math.OC].
- [47] M. Cuturi, in *Advances in Neural Information Processing Systems 26*, edited by C. J. C. Burges, L. Bottou, M. Welling, Z. Ghahramani, and K. Q. Weinberger (Curran, Red Hook, NY, 2013), pp. 2292–2300.
- [48] C. Léonard, *Discrete Contin. Dyn. Syst. Ser. A* **34**, 1533 (2014).
- [49] T. Georgiou and M. Pavon, *J. Math. Phys.* **56**, 033301 (2015).
- [50] Y. Chen, T. Georgiou, and M. Pavon, *SIAM J. Appl. Math.* **76**, 2375 (2016).
- [51] A. Ramdas, N. Trillos, and M. Cuturi, *Entropy* **19**, 47 (2017).
- [52] A. Genevay, G. Peyré, and M. Cuturi, in *Proceedings of the 2018 International Conference on Artificial Intelligence and Statistics* (2018), pp. 1608–1617.

- [53] L. Chizat, G. Peyré, B. Schmitzer, and F.-X. Vialard, *Math. Comput.* **87**, 2563 (2018).
- [54] W. E. Deming and F. F. Stephan, *Ann. Math. Stat.* **11**, 427 (1940).
- [55] R. Sinkhorn, *Ann. Math. Stat.* **35**, 876 (1964).
- [56] R. Sinkhorn and P. Knopp, *Pac. J. Math.* **21**, 343 (1967).
- [57] J. Benamou, G. Carlier, M. Cuturi, L. Nenna, and G. Peyré, *SIAM J. Sci. Comput.* **37**, A1111 (2015).
- [58] A. Genevay, M. Cuturi, G. Peyré, and F. Bach, in *Advances in Neural Information Processing Systems 29* (Curran Associates, Inc., Red Hook, NY, 2016), pp. 3440–3448.
- [59] G. Carlier, V. Duval, G. Peyré, and B. Schmitzer, *SIAM J. Math. Anal.* **49**, 1385 (2017).
- [60] P. Dvurechensky, A. Gasnikov, and A. Kroshnin, in *Proceedings of the 35th International Conference on Machine Learning* (2018), pp. 1367–1376.
- [61] K. Pham, K. Le, N. Ho, T. Pham, and H. Bui, [arXiv:2002.03393](https://arxiv.org/abs/2002.03393) [cs.CC].
- [62] J. Kosowsky and A. Yuille, *Neural Netw.* **7**, 477 (1994).
- [63] P. Koehl, M. Delarue, and H. Orland, *Phys. Rev. Lett.* **123**, 040603 (2019).
- [64] P. Koehl, M. Delarue, and H. Orland, *Phys. Rev. E* **100**, 013310 (2019).
- [65] E. Anderson, Z. Bai, C. Bischof, J. Demmel, J. Dongarra, J. Du Croz, A. Greenbaum, S. Hammarling, A. Mckenney, and D. Sorensen, *LAPACK: A portable linear algebra library for high-performance computers*, Tech. Rep. CS-90-105 (Computer Science Dept. University of Tennessee, Knoxville, TN, 1990).
- [66] A. Bronstein, M. Bronstein, A. Bruckstein, and R. Kimmel, *Int. J. Comput. Vis.* **78**, 67 (2008).
- [67] E. Rublee, V. Rabaud, K. Konolige, and G. Bradski, in *Proceedings of the 2011 IEEE International Conference of Computer Vision (ICCV)* (2011), pp. 2564–2571.
- [68] J. Gower and G. Dijkstra, *Procustes Problems* (Oxford University Press, Oxford, 2004).
- [69] F. Pomerleau, F. Colas, and R. Siegwart, *Found. Trends Rob.* **4**, 1 (2013).
- [70] H. Zhu, B. Guo, K. Zou, Y. Li, K.-V. Yuen, L. Mihaylova, and H. Leung, *Sensors* **19**, 1191 (2019).
- [71] P. Besl and N. McKay, *IEEE Trans. Pattern Anal. Mach. Intell.* **14**, 239 (1992).
- [72] C. Zhu, R. Byrd, P. Lu, and J. Nocedal, *ACM Trans. Math. Softw.* **23**, 550 (1997).
- [73] F. S. Grassia, *J. Graphics Tools* **3**, 29 (1999).
- [74] M. Wright, Interior methods for constrained optimization, in *Acta Numerica* (Cambridge University Press, Cambridge, 1992), pp. 341–407.
- [75] F. Méholi, in *Eurographics Symposium on Point-Based Graphics* (2007), pp. 81–90.